POLITECNICO DI MILANO

Scuola di Ingegneria Industriale e dell'Informazione

Corso di Laurea Magistrale in Materials Engineering and Nanotechnologies

Correlation between morphological, structural and functional properties of nanostructured Aluminum-doped Zinc Oxide films

Relatore: Prof. Andrea LI BASSI

Correlatore: Ing. Paolo GONDONI

Tesi di Laurea di:

Marco DIANI

Matricola 770487

Anno Accademico 2012-2013

To mom and dad...

A mamma e papà...

"Stay hungry, stay foolish"

Steve Jobs

Contents

List of Figures

List of Tables

Abstract

Transparent Conducting Oxides (TCOs) are wide band-gap semiconductors that have, after heavy doping, good electrical conductivity properties combined with high optical transparency in the visible range. New generation photovoltaic devices use these materials mainly as transparent electrodes but the request for cheaper and low environmental impact solutions moved the attention of research to new TCOs like Aluminum-doped Zinc Oxide (AZO). In this work correlation between morphology, structure and functional properties of this material have been studied for nanostructured films deposited using Pulsed Laser Deposition (PLD) that allows to obtain samples with different structure (i.e. doping, defects, nanoscale crystallinity, mesoscale morphology) simply changing oxygen pressure in the chamber during deposition. In order to better investigate the structure-properties relation and in view of an improvement of the functional properties, selected samples have been thermally annealed in high vacuum or argon atmosphere in order to induce crystalline changes in the material structure in the absence of oxygen, since oxygen vacancies play a fundamental role in determining functional properties. Morphology and structure were investigated with Scanning Electron Microscopy, X-Ray Diffraction and Raman spectroscopy while functional properties have been studied using Van der Pauw method (resistivity), Hall effect (mobility and carrier density) and a NIR-Vis-UV absorption spectroscopy (optical). Strong correlation between these properties was observed and some hypothesis to discuss the results are presented.

Sommario

Gli ossidi trasparenti conduttivi (TCO) sono semiconduttori ad ampio gap che, dopo forte drogaggio, presentano buone proprietà di conduzione elettrica insieme ad un'alta trasparenza ottica nel visibile. I dispositivi fotovoltaici di nuova generazione usano questi materiali principalmente come elettrodi trasparenti ma la richiesta di soluzioni più economiche ed a a basso impatto ambientale muovono l'attenzione della ricerca verso nuovi TCO come l'ossido di zinco drogato con alluminio (AZO). In questo lavoro sono state studiate le correlazioni tra morfologia, struttura e proprietà funzionali di questo materiale per film nanostrutturati depositati tramite Pulsed Laser Deposition (PLD), la quale permette di ottenere campioni con strutture differenti (drogaggio, difetti, cristallinità alla nanoscala, morfologia alla mesoscala) semplicemente cambiando la pressione di ossigeno in camera durante la deposizione. Per meglio investigare le relazioni fra struttura e proprietà ed in vista di un miglioramento delle proprietà funzionali, alcuni campioni selezionati sono stati sottoposti ad un trattamento termico di *annealing* in alto vuoto o in atmosfera di argon in modo da indurre cambiamenti nella cristallinità in assenza di ossigeno in quanto le vacanze anioniche giocano un ruolo fondamentale nel determinare le proprietà funzionali. Morfologia e struttura sono state investigate usando un microscopio a scansione elettronica (SEM), diffrazione di raggi X (XRD) e spettroscopia Raman mentre le proprietà funzionali sono state studiate utilizzando il metodo di Van der Pauw (per la resistività), l'effetto Hall (per la mobilità e la densità di portatori di carica) e la spettroscopia in assorbimento NIR-vis-UV (per le proprietà ottiche). Sono state trovate forti correlazioni fra queste proprietà e saranno presentate alcune ipotesi per discutere i risultati.

Introduction

Photovoltaic energy is increasingly used and studied today. This is a direct consequence of downward disponibility of oil simultaneously to the increasing energy demand and a search for sources of clean energy. Different type of photovoltaic cells have been and are now developed. The final goal is to reach systems with low costs and high efficency.
The research on Transparent Conductive Oxides (TCO) lies in this background. They are strongly doped wide gap semiconductors with high transparency to visible light combined with good electrical conductivity. They find use in many new generation photovoltaic cells (inorganic thin film cells, organic and hybrid) as tranparent electrodes or, in particular configuration, as photoanodes but also in others applications as smart windows, touch screens and, generally, in the so called transparent electronics.
Furthermore, nanostructured TCOs with different properties are studied in view of new applications.. So, it is important to study and understand how nanostructuring affects these properties. For instance, it is very important for new photovoltaic applications to create structures able to transport charge along preferential directions and to trap incident light with high scattering nanostructures.
Another goal is to research new materials to reduce costs. A very used TCO is ITO (Indium Tin Oxide) that has high functional properties. The problem is that Indium is a very expensive material due to its shortage on Earth's crust [23]. Furthermore, ITO production is very polluting. One of the goals of recent research is just to substitute indium oxide based materials with cheaper and more sustainable ones. Between these, Aluminum-doped Zinc Oxide is one of the most promising. As a matter of fact, aluminum and zinc

are abundant on Earth's crust and processes used to produce them are green. Aluminum-doped Zinc Oxide (AZO) is a relative new material with some aspects to understand as dopant role, anionic vacancies, scattering mechanisms and properties of nanostructures. Then, research on this material is rapidly developing but still far from that on others TCOs like ITO, studied for several years. In particular, a correlation between structural, electrical and optical properties of AZO is necessary to optimize this material for applications as transparent electrode. It is also important to synthesize this material at low temperature for use in organic or hybrid cells.

Goal of this work is to investigate correlation between morphological, structural and functional properties of nanostructured AZO films not only in view of applications of novel nano or mesostructures (minimize resistivity and maximize transparency) but in particular to understand the relationship between them and how changing ones affects the others. For this reason the investigated samples have very different morphological and structural properties. They have been obtained using Pulsed Laser Deposition (PLD) at room temperature. This technique allows a good control on morphological and structural properties and permits to deposit on different substrates (even plastic). Another important characteristic of PLD is to allow to have different nanostructured films simply changing the pressure in chamber during deposition.

Annealing post-deposition treatments in two different controlled atmospheres were performed for each deposition condition to modify the structural properties of the films. As a matter of fact, it is known that oxygen vacancies play an important role on functional properties. So annealing in oxygen-free atmosphere was done to improve cristallinity without affecting stoichiometry. This can lead to an improvement of properties but also to different structures and this can help to understand relashionships between structure and functional properties. One annealing has been done in high vacuum, the other in argon atmosphere using for both cases an homemade oven.

The morphological characterization of samples was performed by Scanning Electron Microscopy. From resultant images also the films thickness has been evaluated. Structural analysis was performed using X-Ray Diffraction

technique, sensitive to cristallinity of the film, and Raman spectroscopy that gives information about stoichiometry and crystallinity. Electrical measurements were done using Van der Pauw method and Hall effect to obtain films resistivity, carrier density and mobility. Optical analysis (transmittance in the NIR-Vis-UV range) has been done with a spectrophotometer to evaluate optical transparency and haze factor.
At the end of this work also a preliminary annealing experiment in hydrogen-containing atmosphere has been done to evaluate how the presence of this gas may influence functional properties. On these samples only electrical characterization has been carried out so far.
Annealing, electrical measurements and SEM images have been acquired by myself while deposition, Raman spectroscopy and optical analysis with a tutor. XRD has been performed externally from our laboratories at INFN of Milan and analyzed by myself.
This thesis presents this experimental work and a discussion of the obtained results. In particular, Chapter 1 is dedicated to the literature about Transparent Conducting Oxides, their applications (especially in photovoltaic field) and Aluminum-doped Zinc Oxide used as TCO. It also reports information about previous existing works about nanostructured AZO and annealing experiments in different atmospheres. Chapter 2 presents the techniques and experimental set-up used. In particular, the Pulsed Laser Deposition process is introduced underlining its advantages. Then electrical and optical set-up are described with a brief presentation of Scanning Electron Microscopy and X-Ray Diffraction techniques. Finally the annealing procedure is shown. Chapter 3 shows the results concerning morphological, structural, electrical and optical characterization obtained on as-deposited samples, pointing out similarities and differences with literature. In Chapter 4 the results of the annealing experiments are shown and commented. Then there is a comparison between annealed and as-deposited films with a discussion of the obtained results. Finally, Chapter 5 is dedicated to a brief presentation of side or preliminary experiments on AZO, related to this work, and a novel AZO nanostructure is shown.

Chapter 1

Transparent Conducting Oxides

For Transparent Conducting Oxide (TCO) we mean a material in which a high visible light transparency is linked with low electrical resistivity. In this chapter TCO physical properties and applications will be shown, focusing on Aluminum-doped Zinc Oxide (AZO). In particular in section 1.1 electrical and optical properties are shown, in section 1.2 there is a brief discussion about their application in photovoltaic field. Section 1.3 is dedicated to AZO, deposition techniques and its functional properties. Finally, paragraph 1.4 talk about state of art about annealing and section 1.5 explains motivations of this thesis work.

1.1 TCOs functional properties

TCOs are usually semiconductor oxide with wide gap, above 3 eV [1], on which a doping process has been accomplished changing significantly their electrical properties. Usually, this is n-type process, wich leads to good resistivity properties. Instead, p-type TCOs are still in research phase [2][3][4] but they are very studied for their application interest, like in electronic field (diodes made with TCO) [5].
TCOs particular properties make them perfect for transparent electronics like smart windows, flat screen displays and surely in new generations solar cells. In section 1.1.1 there's a presentation of electrical properties of most

common TCOs and section 1.1.2 discuss their optical behavior.

1.1.1 Electrical properties

Figure 1.1 shows band structure of indium oxide In_2O_3, [7], on which a substitional doping with tin oxide SnO_2 has been made forming Indium Tin Oxide (ITO), widely studied in literature. The resultant structure is $In_{2-x}Sn_xO_3$

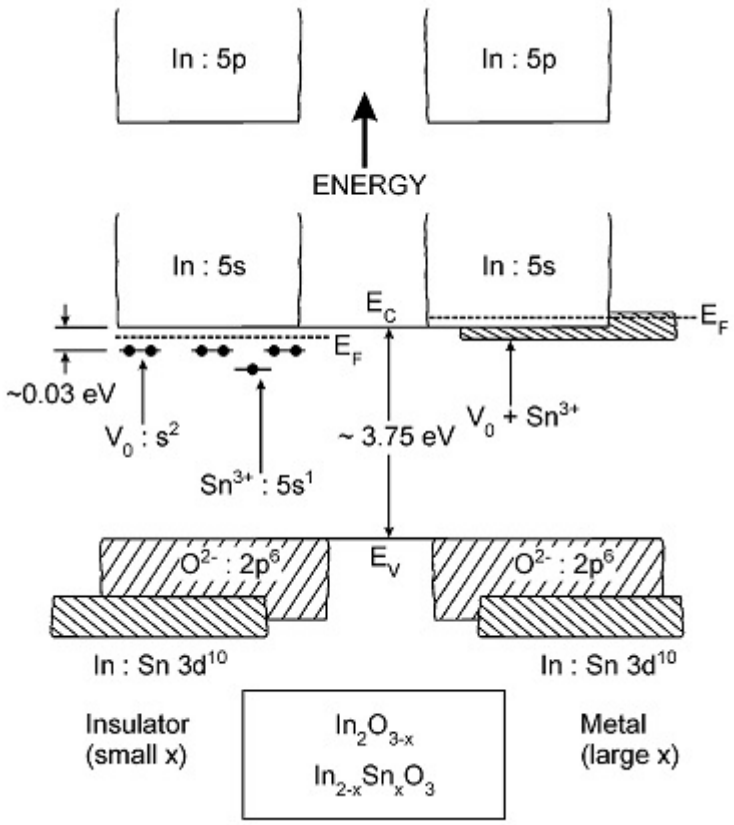

Figure 1.1: Effects of tin doping on indium oxide's band. V_O are oxigen vacancies, x is tin fractions [6].

where x is tin fraction. Tin is tetravalent, so, if In^{3+} is substituted by it,this provides electron in conduction band. Also, with doping, free lattice sites are created in form of oxigen vacancies. 5s orbitals free electrons of In^{3+} are not captured by missing O^{2-} ions creating levels of two electrons per vacancy

near conduction band corresponding to oxygen vacancies (30 meV below it [7]). These defects have low activation energy and good stability [8], so this oxygen substoichiometry is favoured.
In Figure 1.1 on left 5s band of indium is separated from valence band, given by oxygen $2p^6$ band and indium $3d^{10}$, by an energy gap with some levels formed by Sn^{3+} and oxygen vacancies V_O. If doping x increaes, these levels become an energy band full of delocalized electrons near conduction band, giving to the sistem a metallic behaviour. Mott criterium [9] says that a doping threshold exists after which the behaviour is metallic. In this case (ITO) critical density is below 10^{19} cm^{-3} and this value is always overcome in TCOs and so this description of electronic properties is justified. In this way oxide conduction band can be filled without modifing too much energy gap and so transparency. Actually, increasing the carriers density also optical energy gap increases. This effect is called Moss-Burnstein effect and it is shown in section 1.1.2.
Focusing on electric transport properties, it is known that, for a sistem like this, electric conductivity is [10]:

$$\sigma_0 = \frac{ne^2\tau}{m_c^*} = ne\mu \tag{1.1}$$

where

$$\mu = \frac{e\tau}{m_c^*} \tag{1.2}$$

is electrons mobility, e is electron charge and m_c^* is its effective mass in conduction band. So, electrical cnductivity is directly proportional to $n\mu$ product. As discussed in section 1.1.2, absorption in infrared region is proportiona$n$, so carrier density can not be increased too much without affecting optical properties. Therefore, the best way to improve electrical conductivity beyond a certain value of n is to enhance mobility μ. Then, if τ is average time that elapses between two scattering events and i is a specific type of scattering, the Matthiessen's rule says that [11]:

$$\frac{1}{\tau} = \sum_i \frac{1}{\tau_i} \tag{1.3}$$

and, with this formula, mobility can be obtained from equation 1.2.

As already said, there are different scattering mechanisms and, for a TCO,

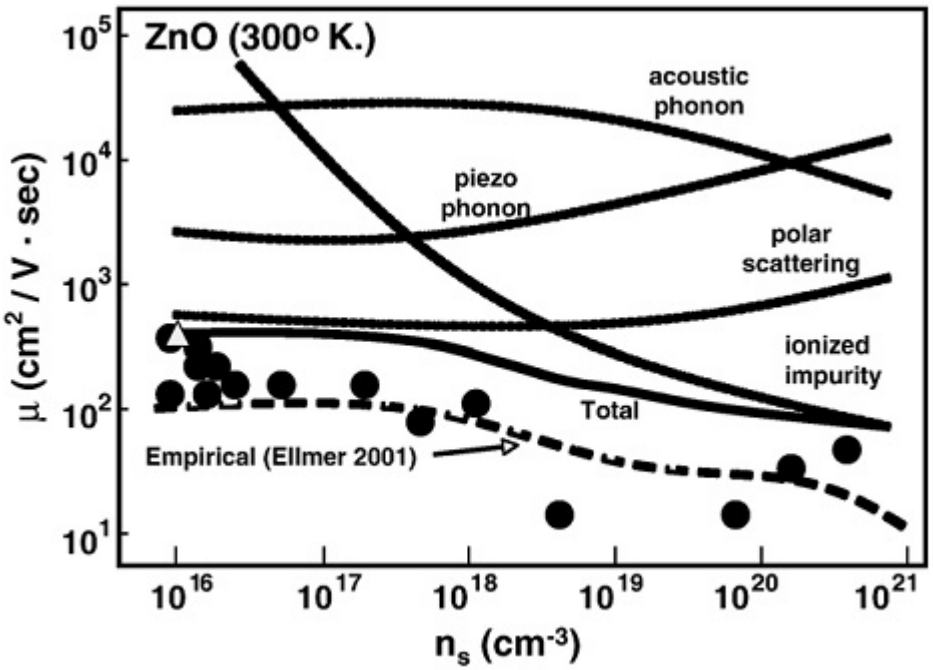

Figure 1.2: Mobility associated to different scattering processes in TCO versus carrier density. Continuous line and triangle are theoretical data, circles are experimental data and spark line is a numerical fitting

they are due to [1][12][13]:

1. Coulombian interaction with ionized impurity (defects or dopant)
2. Polar-optical phonon interaction, that is interaction with lattice vibrations that induce an electrical field due to ionic bond
3. Interaction with acoustic phonons
4. Interaction with dislocations and grain boundaries
5. Interaction with elastic deformation potential of material
6. If crystal is not centrosimmetric, piezoelectric interactions due to deformations

In figure 1.2 [14] mobility versus carrier density is shown. Excluding dislocations and grain boundaries that depend only on structural properties, looking at figure 1.2 it can be deduced that scattering depends stongly on carriers denstity. Over a certain concentration ($10^{19} \div 10^{20}$ cm^{-3}) the dominant mechanism is that with ionized impurity. It is clear that the goal is to act on scattering phenomena that are predominants at not too much high concentration in order to avoid reduction of optical properties, oxygen segregation at grain boundaries and bands distorsion (see figure 1.4 in section 1.2).

1.1.2 Optical properties

A fundamental characteristic of TCOs is their transparency to visible light and also in near infrared and near ultraviolet [15], making them optimal for transparent electronic use.

In visible range, TCO films are characterized by high transparency, usually

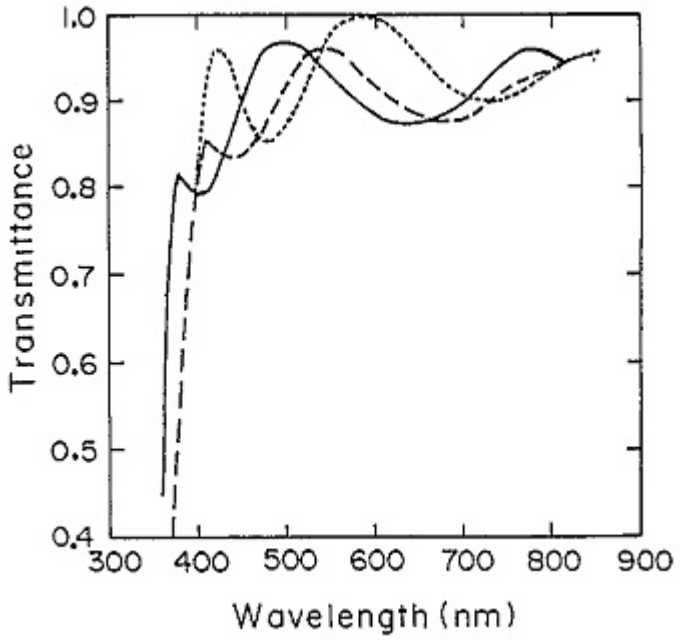

Figure 1.3: Transmittance (in percentage) in visible range by TCOs film with thickness between 250 and 300 nm [16]

more than 90% [1] in which the percentage of transmitted light in function of wavelength presents characteristics interference fringes. This effects depends on film refraction index, film thichness and also on its nanostructure. From these oscillating profiles it is possible to calculate refraction index of these materials [17][18], including imaginary part (related to absorption coefficient), film thickness and average visible transmittance. At higher energy,

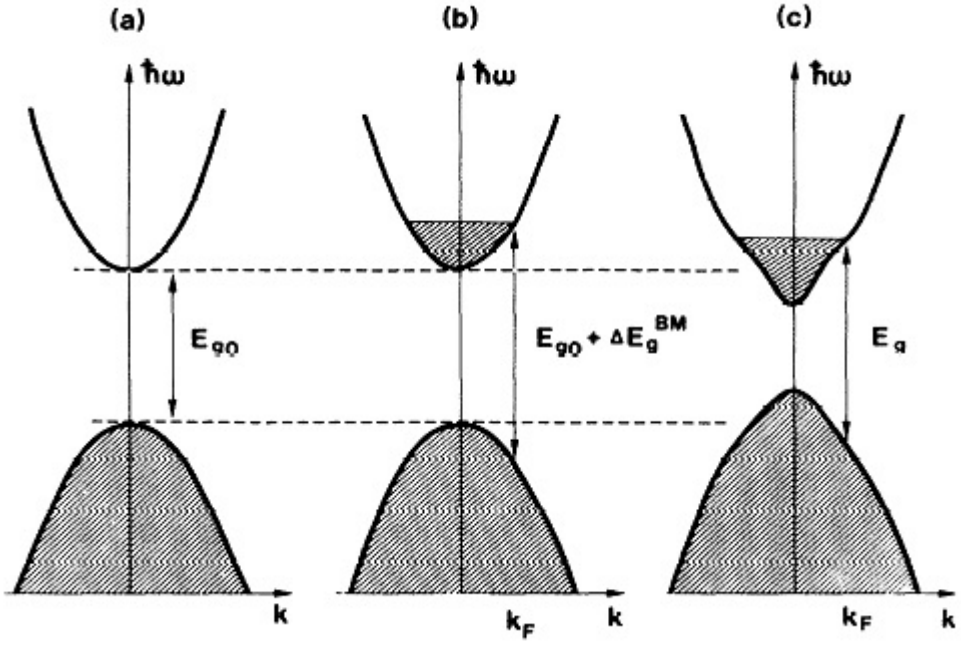

Figure 1.4: Band scheme for (a) an intrinsic semiconductor, (b) degenerate doped with gap increasing due to Moss-Burnstein effect, (c) considering many-body effect [21]

in near ultraviolet region, photons have enough energy to promote an electron from valence band to conduction band. In this way TCO stop to be transparent when photons exceed energy gap. Its amplitude is studied generally with Tauc plot [19], a graphical method that uses absorption material profile nearoptigal energy gap.

It is really important to keep in mind that for a degenerate semiconductor (like TCOs) it is experementally demonstrated that increasing carrier density optical energy gap shows an increase. This effect is known as Moss-Burnstein

effect [20] and it is shown in figure 1.4. It is a consequence of Pauli's exclusion principle. So, the filling of conduction band by free carriers causes the occupation of its bottom. In this way higher energy is needed to promote an electron from valence band. The variation of optical gap is [22]:

$$\Delta E_g = \frac{\hbar^2}{2m^*}(3\pi^2 n)^{\frac{2}{3}} \tag{1.4}$$

with $3\pi^2 n = k_F$ Fermi wave vector. Actually, interactions between electrons oppose to Moss-Burnstein effect and so the increasing in energy gap (ΔE_g) is less than calculated one. This is a consequence of many-body effects and leads also to a band distorsion making wrong bands' parabolic approximation as shown in figure 1.4 (c).

As said before, loss of transparency at low energies is due to absorbance of infrared radiation by free carriers. In section 1.1 it has been explained that carriers due to dopant and oxygen vacancies creates levels near conduction band. Electrons in this band can be modeled as a free electron gas, with average collision time τ, neglecting electron-electron interactions. So, they can collide only with lattice ions (Drude model) [10]. So, if the system interacts with an electromagnetic wave with frequency ω, it exists a plasma frequency ω_p at which the radiation is able to supply a collective oscillation of charge carriers. Defining $\epsilon(\omega)$ as dielectric function of a material and if

$$\omega\tau \gg 1 \tag{1.5}$$

where τ is average time between two collisions, applying Maxwell equations it can be calculated that

$$\epsilon_1 = \epsilon_\infty \left(1 - \frac{\omega^2}{\omega_p^2}\right) \tag{1.6}$$

$$\epsilon_2 = \frac{\epsilon_\infty \omega_p^2}{\omega^3 \tau} \tag{1.7}$$

where

$$\epsilon(\omega) = \epsilon_1(\omega) + i\epsilon_2(\omega) \tag{1.8}$$

with ϵ_∞ dielectric constant at high frequency, ϵ_1 real part of material's dielectric function and ϵ_2 immaginary part. So, it can be defined a collective plasma oscillation as

$$\omega_p = \sqrt{\frac{ne^2}{m_c^* \epsilon_0 \epsilon_\infty}} \tag{1.9}$$

So, plasmonic oscillation depends on carrier density and also absorbed intensity is proportional to n as shown in figure 1.5 [22].

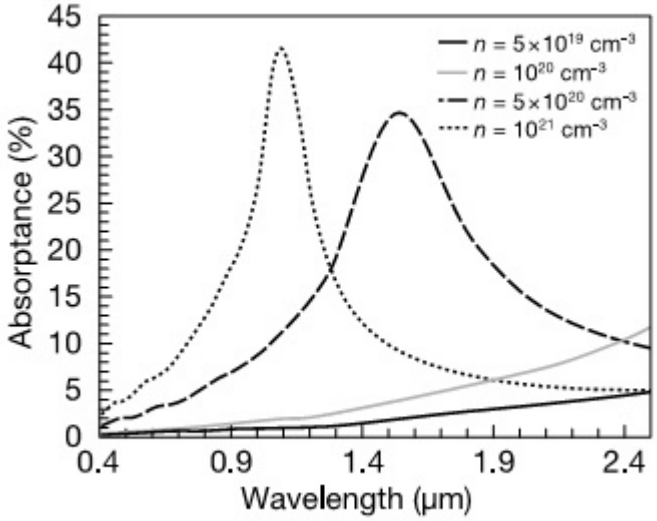

Figure 1.5: Absorption in IR range due to free carriers in TCOs

1.2 Transparent Conducting Oxides in photovoltaics

TCOs are widely used in new generations photovoltaic cells. This is due to their ability to transport current, to maximize photons' collection and to trap light. They have also low environmental impact and new materials are cheap. For example, ITO is very expensive (because fo indium cost) so different materials like Zinc Oxide (ZnO), Aluminum-doped Zinc Oxide (AZO) and Fluorine Tin Oxide (FTO) are used [23].

New generations cells are basically of three type: thin film, organic and hybrid. CIGS ($Cu(InGa)Se_2$) or cadmium telluride (CdTe) cells are based on thin film technology. For these type of cells TCOs are widely used. As shown in figure 1.7 in CIGS solar cells a triple TCOs layer is used, in particular AZO, ZnO and CdS. This coating works as defects passivating material for active zone and reduces also eddy currents to electrodes. In CdTe cells TCO works as anti-diffusive barrier during high temperature deposition of cadmium telluride, keeping good electrical properties.

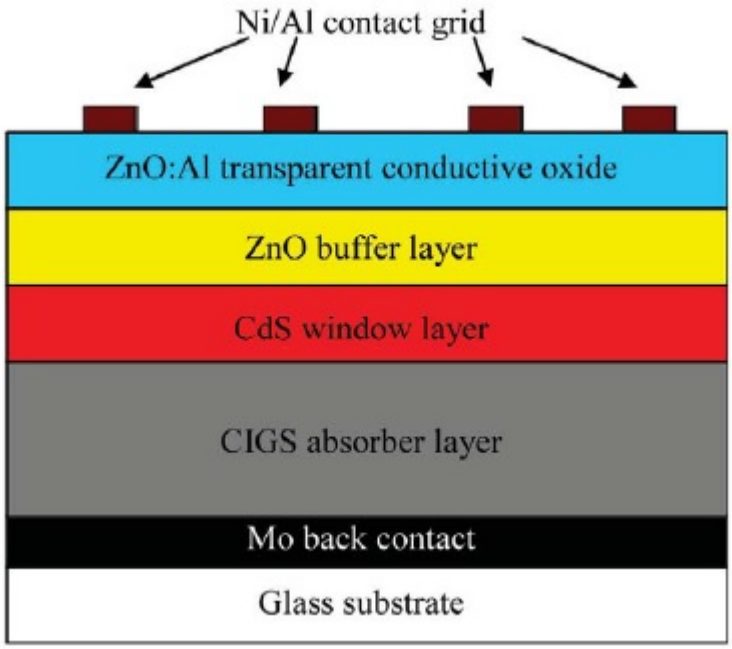

Figure 1.6: Scheme of CIGS cell

Research on TCOs is very important for Gräetzel and organic cells, expecially for the possibility to have nanostructured films. The first one, also called Dye Sensitized Solar Cells (DSSC) are formed by two TCO fim which enclose a nanostructured TiO_2 with a dye coating in an electrolyte solution. Dye absorbs photon giving electrons to the TiO_2 that transport it to the electrode (formed by TCO). Dye oxidized molecules take an electron from the electrolyte, reducing it, which oxidates himself (returning to the starting

point) with electron on counterelectrode (also this made with TCO), coming from external circuit. This operation can be performed indefinitely [25]. It is clear that is very important to increase the interface between TiO_2 (or others inorganic materials) and organic molecules (dye). This can be performed using nanostructures like nanorods in which there is a preferential current transport direction [26] [27]. Titanium dioxide is a polluting material. So, some TCOs as Fluorinated Tin Oxide (FTO) could be used instead of TiO_2. Furthermore, Heterojunction with Intrinsic Thin layer (HIT) is a cell in which active layer is a thin film. In these devices TCO plays role of transparent electrode. In this sistem is very important light trapping ability of cells, improving it with some techniques as texturing in order to increase the mean free path of light in the active layer. A pattern is imposed to TCO during deposition or after with micro and nanolitography to increase haze factor. In these sistem it is important to deposite materials at low temperature because of contact between amorphous silicon n^+ and TCO. In this way photovoltaic cells require less quantity of materials, reducing costs. This property of light trapping is fundamental also for amorphous silicon and Bulk Heterojunction solar cells (BJT).

1.3 Aluminum-doped Zinc Oxide (AZO)

Aluminum-doped Zinc Oxide (AZO) is the material object of this thesis work. Zinc Oxide (ZnO) is a semiconductor with a direct gap of 3.3 meV [28]. It has usually crystalline structure of hexagonal wurtzite type (Figure 1.7) with ionic bond for 62% [29]. Qualitatively, wurtzitic structure is formed by two different interpenetrating sublattices, one formed by zinc ions and the other by oxygen ions. There are four atoms per unit cell that is hexagonal with two lattice parameters, a and c, in the ratio of

$$\frac{c}{a} = \frac{8}{3} = 1.633 \tag{1.10}$$

Without doping, ZnO substoichiometric shows conductivity with a free electron density in the order of 10^{17} cm^{-3}. Doping it with aluminum, ZnO be-

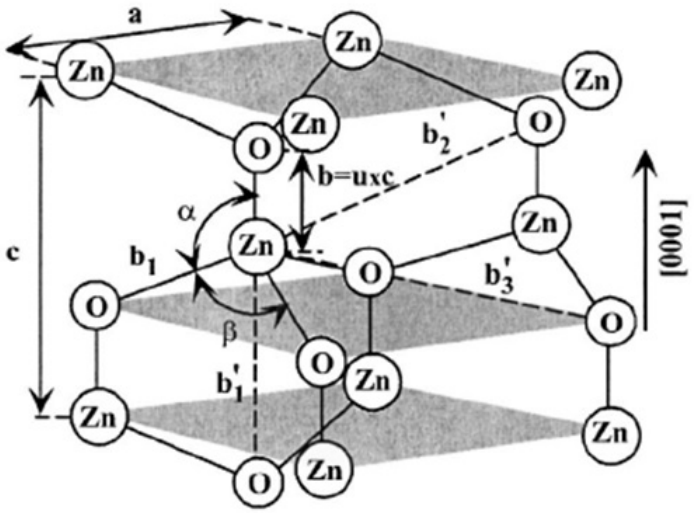

Figure 1.7: Wurtzitic cell of zinc oxide.

comes conductive. In fact, substitution of Zn^{2+} ions with Al^{3+} and creation of oxygen vacancies create free electrons states near to conduction band (see section 1.1.1). Free electrons density of AZO can reach order of 10^{23} cm^{-3} [24]. Increasing doping causes a negative effect as seen in sections 1.1.1 and 1.1.2: mobility reduces due to more probable scattering events and transparency window reduces (due to plasmonic effect). It has been found that the optimal concentration of aluminum is 2% wt [30]. Resistivity values of the order of 10^{-4} Ωcm and transparency values higher than 90% have been reported [24] [14] [31]. It is a very interesting material because it is indium free. Furthermore, aluminum and zinc are abundant on Earth's crust.

TCOs, and in particular AZO, can be deposited using different techniques divided in two main categories. First one includes deposition techniques with chemical precursors as CVD or pyrolysis, second one by solid target erosion (Physical Vapor Deposition) as Magnetron Sputtering (MS) and laser ablation.

Deposition techniques through chemical precursors used in TCOs production are basically Chemical Vapor Deposition through metallorganic compounds (MOCVD) and spray pyrolysis (CSP). For both cases film is obtained as a result of a surface reaction between the precursors. The main difference

Table 1.1: Comparison between different resistivity obtained with different materials and deposition techniques [14]

Material	Deposition technique	Resistivity (10^{-4} Ωcm)
AZO	PLD	0,85
AZO	PLD	1,39
ITO	PLD	0,95
ITO	MS	1,2
Mo:In_2O_3	MS	1,6
ITO	CSP	0,77
Mo:In_2O_3	MS	1,5

is that they are in vapor phase for MOCVD and as pyrolyzed powders for CSP. These techniques allow a good control on structural properties [32] but films obtained could have low electrical and optical performance [33][34]. Magnetron Sputtering is a Physical Vapor Deposition (PVD) technique. A collimated (with a magnetic field) beam of Ar^+ ions impacts on a solid target ablating atoms that deposit on a selected substrate. Approximately 33% of deposited TCOs for research purpose is done with MS. As a matter of fact with radio frequency Magnetron Sputtering (most used than DC MS) it is possible to create films with large surface area and to have a good control on growth rate. So, through this parameter also films structure and performance can be controled.

The deposition technique used in this thesis work is Pulsed Laser Deposition (PLD), a physical vapour deposition method which permits to deposit at environmental temperature or also with hot substrates. A laser impacts on a solid target in a vacuum chamber (that can be filled with a gas controlled in pressure) causing ablation of it. So, ablated species move to substrates were they deposit creating a film. It is important now to underline a peculiar characteristic of this method: the possibility to deposit with different pressure in chamber. As a matter of fact, depositing at low gas pressure (in this case oxygen), species ablated have high kinetic energy so, when they impact on substrates they can move and reorganize themselves, creating a

compact film. On the contrary, if oxygen pressure is high (more than 100 Pa), clusters and nanoparticles can nucleate in the gas phase and deposit with low kinetic energy. In this case, they can not move and the resulting structure is hierarchical [35]. Generally, films obtained with PLD have better electrical properties than that obtained with other deposition techniques. A comparison between different resistivity obtained with different materials and deposition techniques is in Table 1.1 [14].

In Figure 1.8 cross-section of AZO films obtained with Pulsed Laser De-

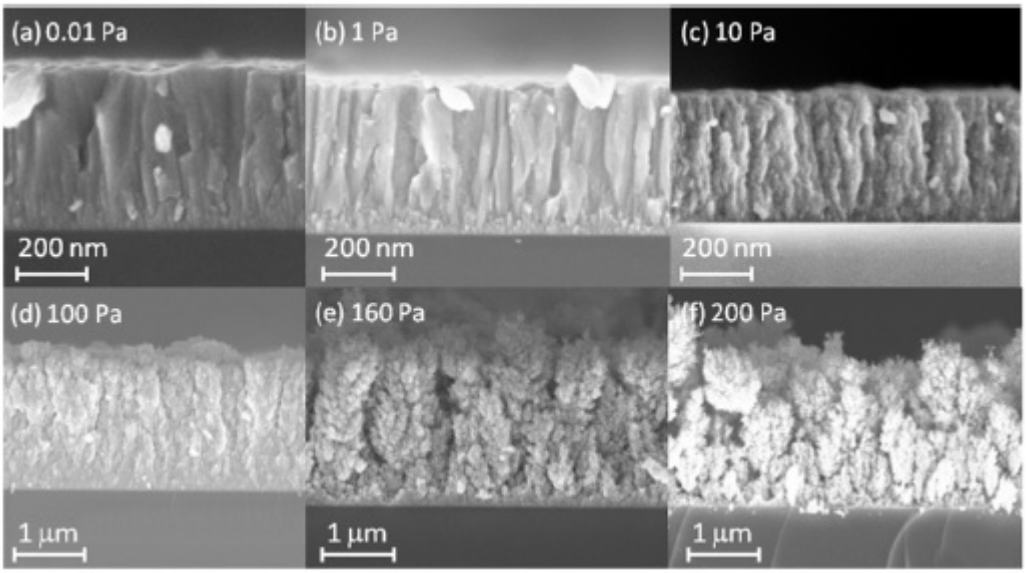

Figure 1.8: Scanning Electron Microscope (SEM) images for AZO films deposited at different pressure [24].

position with different pressure are shown. The images are obtained with a Scanning Electron Microscope. It is visible that increasing pressure morphology changes from compact to porous. Compact films are very conductive, porous films have good scattering properties. A hierarchical structure in fact has a high haze factor, better scattering light [24][36].

1.3.1 Structure of Aluminum-doped Zinc Oxide films

AZO films deposited with PLD strongly present (002) peak of the ZnO wurtzite structure, revealing a preferential (002) growth direction, although

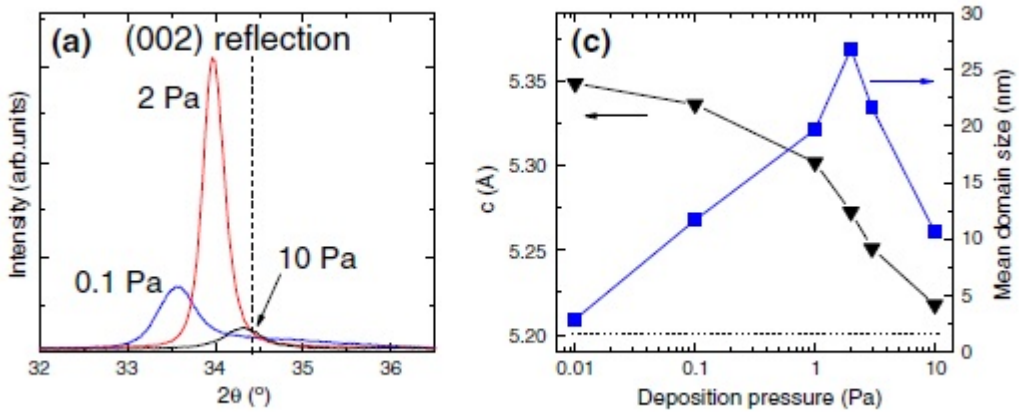

Figure 1.9: (002) peak for AZO films (left) at different deposition pressure and mean domain size and lattice parameter (right). [36].

for these films the peak is shifted with respect to the reference position of the ZnO (002) reflection (34.44°), as can be seen in Figure 1.9 (left) [36]. From 0.01 Pa to 1 Pa the diffraction feature is broad, asymmetric and weak, indicating a high degree of disorder, probably due to an excess of oxygen vacancies. As the pressure increase, also the intensity of the (002) reflection increases, reaching a maximum at 2 Pa, then starts to decrease. At 10 Pa the (002) peak is still dominating, but other diffraction peaks appear, indicating that the film includes (002) oriented domains together with an assembly of randomly oriented nanosized crystal grains.
Using Bragg's law and Scherrer formula (see Section 2.4) also vertical lattice parameter c and mean domain size D can be calculated (see Figure 1.9 right). From this plot it is clear that the optimal case is for the film deposited at an oxygen pressure of 2 Pa. This could be due to the fact that deposition at low oxygen pressure gives films with a large amount of oxygen vacancies, possibly affecting the correct position of Zn^{2+} ions in the lattice, and with Al^{3+} ions not occupying substitutional sites. Moreover the large deposition kinetic energy also results in the presence of high stress. As the pressure is increased to 10 Pa, oxygen vacancies are reduced and aluminum ions occupy lattice sites instead of interstitial positions, but the crystalline order

decreases probably because of the effect of the background gas which favors cluster nucleation in the plasma plume and reduces kinetic energy of ablated species [36].

1.3.2 Electrical properties of Aluminum-doped Zinc Oxide films

As seen in section 1.1.1 conductivity can be wright as

$$\sigma = nq\mu \tag{1.11}$$

Besides, changing oxygen pressure in PLD chamber modifies the resulting

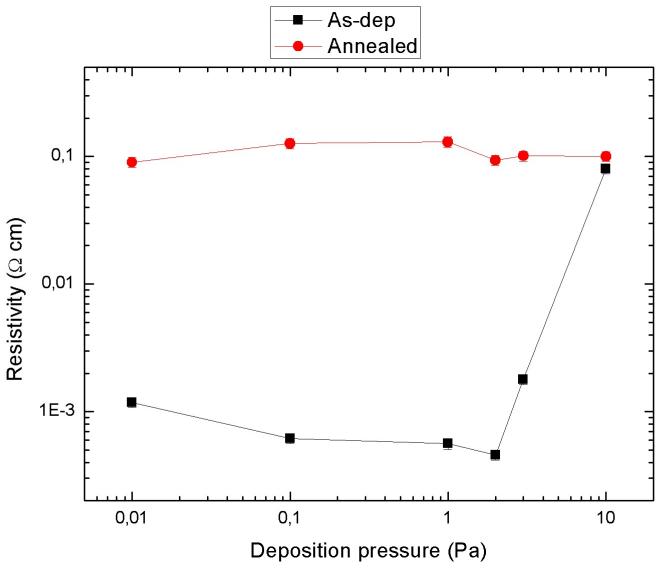

Figure 1.10: Resistivity of AZO films for different oxygen pressure. Black squares are as deposited samples, red circle are annealed samples [24].

structure (and so mobility) but also carrier density. As a matter of fact, depositing at low pressure creates more oxygen vacancies with respect to high pressure deposition. So structure influences very strongly electrical properties. Figure 1.10 [24] shows resistivity (in Ωcm) as a function of deposition pressure (in Pa). Black squares are as-deposited samples, red circle are sam-

ples subjected to an annealing process in air to understand role of anionic vacancies. As a matter of fact, during the heating, vacancies are filled with oxygen present in the atmosphere, demonstrating that an important part of charge carriers is due to it (see figure 1.10). It has been found [24] that the

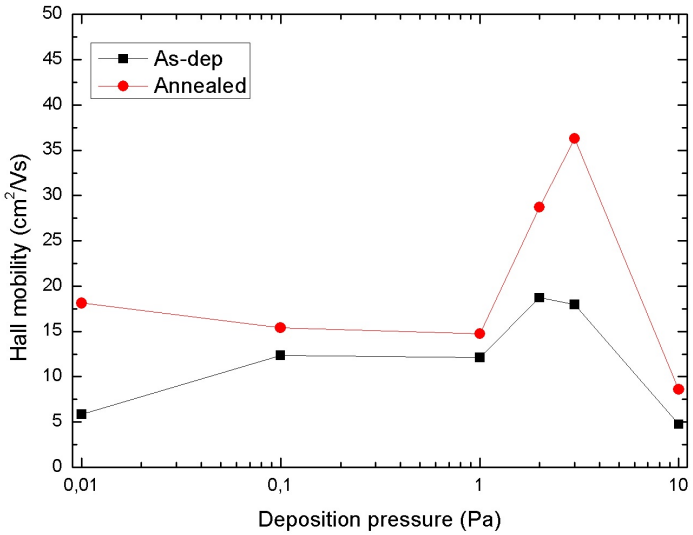

Figure 1.11: Hall mobility of AZO films for different oxygen pressure. Black squares are as deposited samples, red circle are annealed samples [24].

optimal oxygen pressure is 2 Pa (see figure 1.10) at which resistivity reaches a value of the order of 10^{-4} Ωcm.
Mobility is shown in figure 1.11. Also in this case the optimum is for 2 Pa oxygen pressure. It is very interesting to observe that after annealing mobility improves. This is due to a reorganization of nanodomains that form during deposition but also to a desorption of oxygen at grain boundaries that works as trap site. Carrier density, on the contrary, decreases after annealing in air proving that it is due not only to electrons from substitutional Al^{3+} ions but also from oxygen vacancies (see figure 1.12).

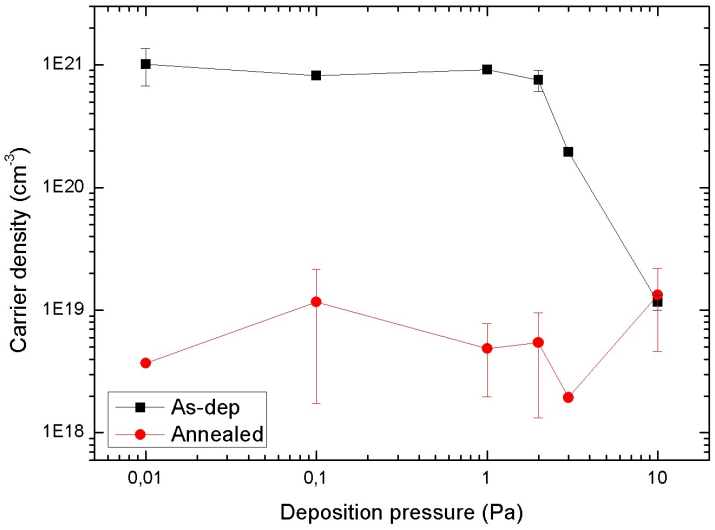

Figure 1.12: Free carrier density of AZO films for different oxygen pressure. Black squares are as deposited samples, red circle are annealed samples [24].

1.3.3 Optical properties of Aluminum-doped Zinc Oxide films

In figure 1.13 [24] optical transmittance properties for different deposition pressure are shown. At low pressure (up to about 10 Pa) films present high transparency in visible range and a strong transmittance reduction in infrared. This is due to plasmonic absorption at these wavelengths, as shown in section 1.1.2. This effect decreases with increasing pressure because also free carrier density decreases as seen in section 1.3.1. Compact and porous films differ also near the optical gap. The second ones have sharper profiles than first ones and a shorter extension in wavelengths. This is due to a considerably lower number of defect states below conduction band for porous films. Some interferences fringes can be seen for compact films that disappear for porous ones. In fact, porous film presents a high degree of morphological disorder that does not allow optically coherent phenomena.
In figure 1.14 mean haze factor (in percentage) as a function of deposition pressure is shown [24]. It is clear that at high pressure haze factor strongly

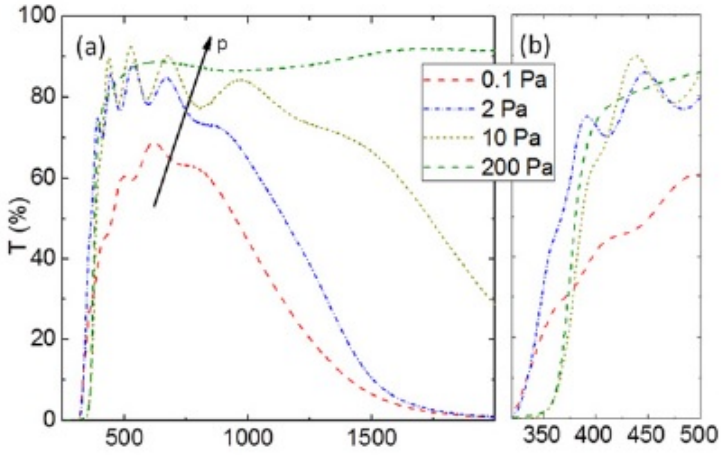

Figure 1.13: Percentage of transparency of AZO films at different oxygen pressure [24].

increases. This is due to morphology of these films. As a matter of fact, for pressure higher than 10 Pa structure becomes hierarchical and if, cluster dimension is comparable with incident light, this configuration has a strong scattering power, trapping light very easily. The ratio between scattered light and total transmitted light is called haze factor.

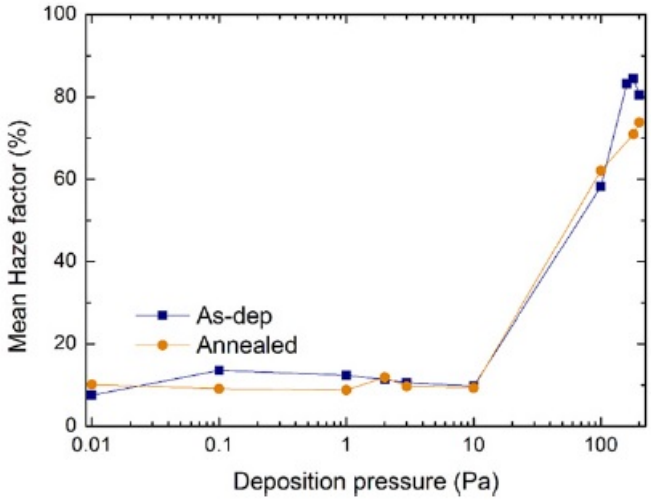

Figure 1.14: Mean haze factor (in percentage) at different oxygen pressure [24].

1.4 Annealing of AZO samples

Annealing is a post deposition thermal treatment that can improvematerial properties and can be also used to understand some phenomena and behavior nature. For AZO different studies are present in literature. An important procedure is annealing with n-type amorphous silicon (a-Si) capping layer in nitrogen atmosphere [37] [38] [39]. This device is used to prevent elctrical properties deterioration due to oxygen presence, forming a barrier to its diffusion. AZO films were prepared with DC magnetron Sputtering with optimized deposition conditions so that AZO films exhibited a good surface roughness for light scattering and low resitivities. The resulting films are compact with thickness of about 900 nm.
Uncapped AZO films annelaed in nitrogen atmosphere show a behavior like that in figure 1.15 [37]. It is clear that for increasing annealing time, carrier

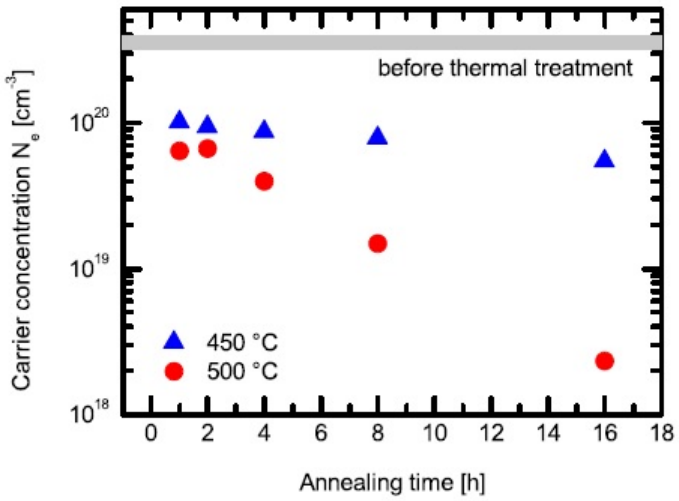

Figure 1.15: Carrier density of AZO films after annealing in nitrogen atmosphere versus annealing time [37].

concentration decreases. This is due to deterioration action of oxygen present in the atmosphere, effect that grows at high temperature.
To prevent oxygen migration into the film, a capping layer can be deposited on films. Different capping layer have been studied and the best is silicon

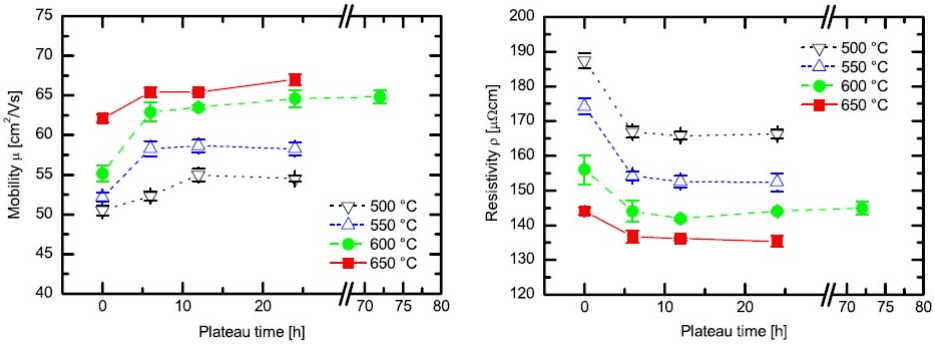

Figure 1.16: Mobility (left) and resistivity (right) in function of annealing time at different temperature [37].

with thckness more than 40 nm [37] [38]. It has been deposited by Plasma Enhanced Chemical Vapor Deposition (PECVD) and obtained samples have been annealed at temperature of 600 °C (common temperature for crystallization of amorphous silicon). Silicon thickness is important not only to create a barrier against oxygen but it has also a strong influence on the mechanical stability of the layer stack upon annealing. Samples with silicon capping layer too thin present in fact cracks that could appear also few days after thermal treatment. Besides, films with thinner capping layer (15 nm) show a reduction of carrier concentration for long time annealing due to oxygen migration into the film. Results about Hall mobility and resistivity are

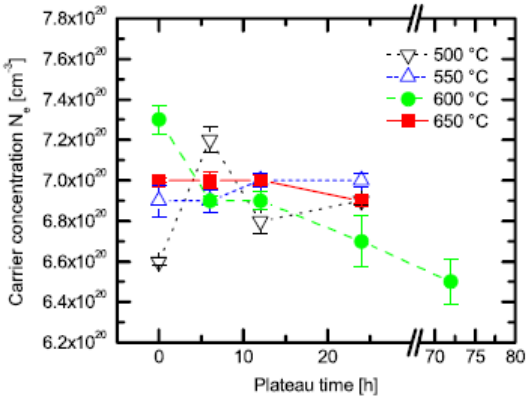

Figure 1.17: Carrier density in function of annealing time at different temperature [37].

shown in Figure 1.16 [37]. Before annealing initial mobility is of 42 cm^2/Vs and starting resistivity is around 270 $\mu\Omega$cm. It is evident that these two quantities improve till 6 hours annealing time and then they stabilize, reaching higher values with higher temperature. This is main due to a reduction of defects at the grain boundaries but also to a decrease of neutral impurities and crystallographic defects as dislocation [37] [38]. An increasing in carrier density nearly instantaneous and a decreasing of it after 6 hours *plateau* were observed as shown in Figure 1.17. This effect can be explained considering capping layer. Further carriers can originate from it, exactly from the migration of hydrogen contained in it to AZO film.
Optical properties after thermal degradation and a consequent annealing with capping layer were studied in a different paper [38]. It has been observed that the maximum of absorption in infrared, due to plasma oscillations of the free charge carriers in the film, is shifted to longer wavelenths after thermal degradation and then shifts back after annealing under capping layer (Figure 1.18). This is due to loss of free carriers during first process and an increase in carrier density during second process.

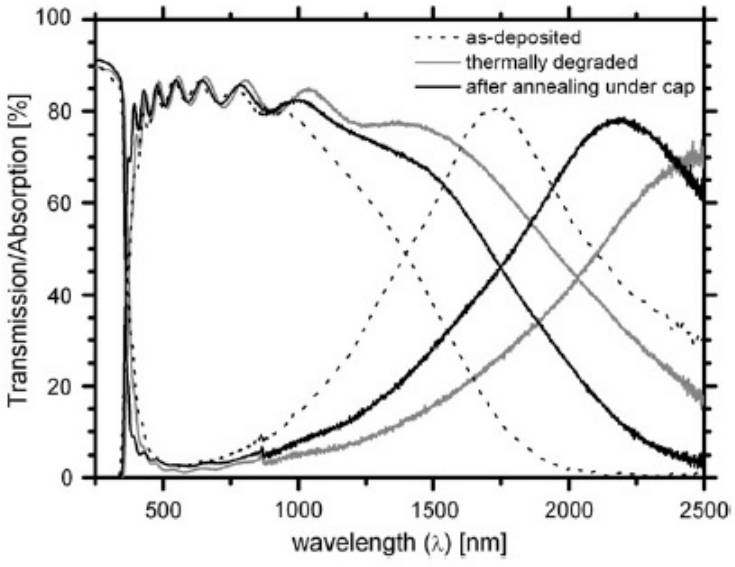

Figure 1.18: Transmission and absorption of AZO films in function of wavelength [38].

Another type of annealing used in some papers can be done in vacuum or controlled atmosphere. In this case oxygen into the film can be reduced [41]. This has been done in a work on Gallium-doped Zinc Oxide (GZO) whose results are shown in figure 1.19 (left). In this case a slight increase in carrier density was obtained. A great improvement on the contrary has been reached for Hall mobility. To improve also carrier concentration a thermal treatment in hydrogen atmosphere can be done [40]. In this case gas diffuses into the film increasing a lot free carriers (figure 1.19 right), enhancing also Hall mobility (through reduction of defects at grain boundaries and reorganization of nanodomains).

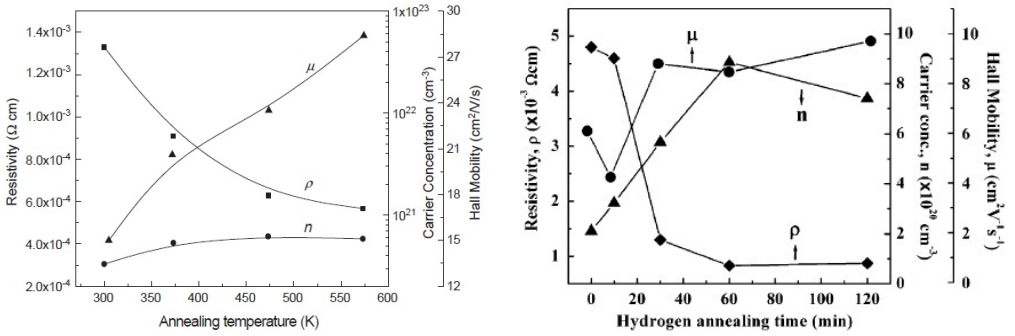

Figure 1.19: Resistivity, Hall mobility and carrier concentration for annealing in vacuum (left) [41] and in hydrogen atmosphere (right [40])

1.5 Aims of this work

This thesis work is framed in the above presented context. Its aim is to study the interconnection between structural and functional properties and to explore the possibility to improve the second ones acting on the first ones. To do this, two different sample series have been deposited through Pulsed Laser Deposition at different oxygen pressure, the first series at 0,1, 2, 5, 10, 50 and 100 Pa and the second series only at 0,1, 2, 10, 100 Pa. Then, a sample for each deposition condition has been annealed in two different atmospheres, high vacuum and argon, at 500°C for 1 hour. All of them have been analyzed in cross-section and from above with Scanning Electron Microscope to study

their morphology. On the first series electrical measurements have been performed to calculate in plane resistivity, Hall mobility and carrier density and optical measures to evaluate transmittance and Haze factor. Films of the second series have been deposited with a higher tickness to study structural properties through Raman spectroscopy and X-Ray Diffraction in addition to electrical measurement.
These analysis were performed to investigate which correlations exist between structure and functional properties. In particular, the ultimate goal of this research approach is to understand the role of stoichiometry, oxygen vacancies, substitutional ions, defects, nanocrystallinity, grain boundaries, mesoscale morphology and how these characteristics affect electronic and optical properties, in view of the development of materials with enhanced performance. As discussed in the following chapters, the results here presented also leave open questions to be addressed by future experiments.

Chapter 2

Techniques and experimental set-up

In this chapter strumental set-up and techniques are presented. In paragraph 2.1 there's a brief discussion about deposition procedure, section 2.2 and 2.3 shows instruments used for morphological and structural anlysis. Paragraph 2.4 it's a deepening on electrical measurements and in section 2.5 is shown the experimental set-up of optical measurements. Finally, section 2.6 shows annealing procedure.

2.1 Pulsed Laser Deposition

All sample were deposited by Pulsed Laser Deposition (PLD) on glass and silicon (100) substrates. First ones are optimal for Scanning Electron Microscope analysis while glass substrates are used for XRD,Raman, electrical and optical properties due to their transparency and high resistivity. PLD is a physical vapor deposition technique based on the production of a plasma from a material target irradiated by intense laser pulses, making this instrument perfect for depositing a wide range of materials such as metals, ceramics and even oxides [35].
The general operation scheme for PLD is shown in figure 2.1. In particular, in this work, a Nd:YAG pulsed laser frequency-quadrupled, with $\lambda = 266$ nm,

is focused on a solid target composed by sintered powders of ZnO and Al_2O_3 2% in weight. Pulses have 10 Hz repetition rate, 6 ns duration time, 75 mJ energy and a fluence (energy density) of about 1 Jcm^{-1}. The laser interacts with the target surface causing the ablation of particles and aggregates that expandes in form of plasma plume to the substrates.

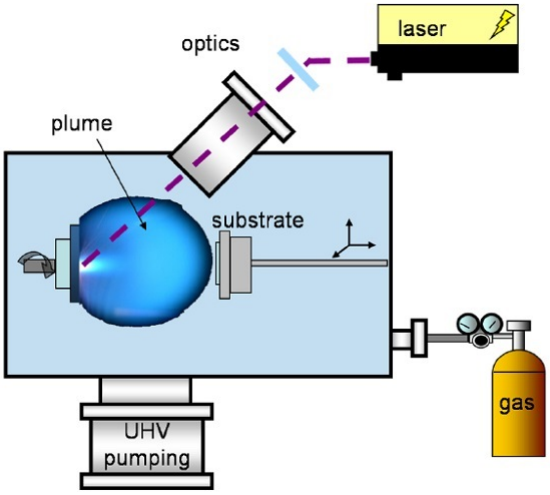

Figure 2.1: Scheme of PLD apparatus [42]

In sinthesis the procedure is this:

1. The substrates are cleaned and placed in the vacuum chamber.
2. When a certain low pressure in the chamber ($p \approx 3 \cdot 10^{-3}$ Pa) is reached, a gas (in this case oxigen) is introduced with a controlled pressure.
3. Substrates are misaligned (see Figure 2.2) and put in rotation. In this way the deposited thickness is more uniform.
4. The laser is focused on the rotating target and the plasma plume forms.

Some parameters are very important in this process like the distance between target and substrates and the type of background gas or mixture that influence kinetic energy of ablated species. In this work what has been changed

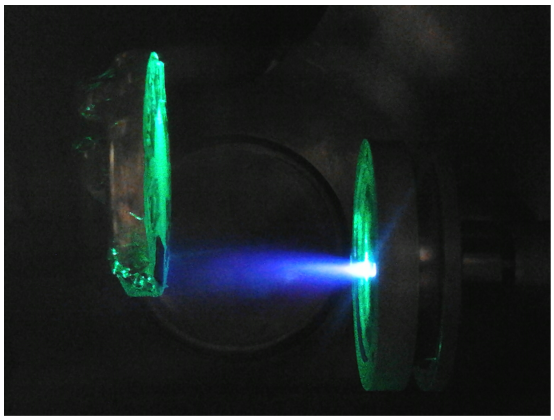

Figure 2.2: Scheme of PLD apparatus [42]

for different samples is the partial oxygen pressure. If this value is low, ablated species have a high kinetic energy. So, when they impact on substrates, they can reorganize and the resultant film is compact and more crystalline. On the contrary, if the oxygen pressure is high the species have a low kinetic energy with a consequent low superficial mobility and the resultant structure are disordered and more hyerarchical. Furthermore, a higher oxygen pressure leads to the formation of clusters with a low superficial mobility resulting in cluster-assembly growth. All depositions were made at room temperature.

2.2 Scanning Electron Microscope

A scanning electron microscope (SEM) is a type of electron microscope that produces images of a sample by scanning it with a focused beam of electrons. They interact with atoms in the sample, producing various signals that can be detected and that contain information about the sample morphology. The most common detection mode is collecting secondary electrons emitted by atoms excited by the electron beam. The number of this secondary electrons is a function of the angle between the surface and the beam.So, scanning the sample, an image displaying the morphology of the surface is created.
In this work a Field emission Zeiss Scanning Electron Microscope (model 40) have been used to aquire cross-section and surface images.

2.3 X-Ray Diffraction and Raman spectrometer

X-Ray Diffraction is a technique used for determining the atomic and molecular structure of a crystal. Crystalline atoms cause diffraction of an incident X-rays beams into many specific directions that are described by Bragg's law that says that

$$2dsin(\theta) = m\lambda \tag{2.1}$$

where d is the distance between two adjacent planes, λ is wavelength of incident radiation (in this case 1,54 Å) and θ is the angle that incident radiation forms with crystalline plane. So, an XRD spectrum is formed by different peaks at θ positions. Considering vertical reflections vertical lattice parameter c can be calculated.
Analyzing XRD spectra also mean domain size D can be estimated. As a matter of fact, Scherrer formula says that

$$D = \frac{0,9\lambda}{\beta cos(\theta)} \tag{2.2}$$

where β is Full Width at Half Maximum (FWHM) of one peak, θ is the position (in degree) of the same peak and λ is X-Ray wavelength.
XRD spectra have been acquired with a diffractometer working in reflection mode and 2θ configuration in an interval of 20-80° with radiation Cu $K_{\alpha 1}$ with λ = 1,5406 Å.
For Raman analysis a InVia Raman spectrometer with excitation wavelength of 457 and 532 nm and a resolution of 3 cm^{-1} have been used.

2.4 Electrical measurements

2.4.1 Resistivity measurements

Electrical measurements on thin films have been performed using Van der Pauw method. The experimental configuration is shown in figure 2.3. It is a

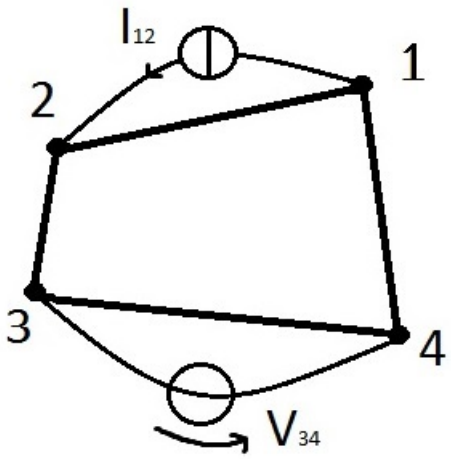

Figure 2.3: Experimental configuration for Van der Pauw measurements

four contact scheme proposed by Van der Pauw in 1958 [43] that enable to calculate sheet resistance of arbitrarly shaped thin films injecting a current between two contacts and measuring voltage drop between the other two. If we suppose to force a current I_{12} from contact number 1 to contact number to 2 and to measure the voltage drop V_{34} between contact 3 and contact 4, we can define

$$R_{12,34} = \frac{V_{34}}{I_{12}} \tag{2.3}$$

Now, if these hypotesis are true

1. Film thikcness is uniform
2. Contacts are on sample edges
3. $\frac{D}{L}$ is small where D is contact diameter and L is the distance between them
4. Sample surface is simply connected (no isoleted region are present)

we can introduce also the sheet resistance R_S that is the resistance per thickness unit measured in $\Omega/\square$ and the Van der Pauw equation is true (independently from sample's shape)

$$e^{-\pi \frac{R_{12,43}}{R_S}} + e^{-\pi \frac{R_{23,41}}{R_S}} = 1 \tag{2.4}$$

and consequently the resistivity ρ is simply defined as

$$\rho = R_S d \tag{2.5}$$

where $R_{23,41}$ is defined in the same way of $R_{12,43}$ and d is the film thickness. Measurements have been performed on all possible injected current - measured voltage configurations so that we can average them. Configurations with same current in two different directions are considered different. Clearly, for reciprocity theorem is

$$R_{21,34} = R_{12,43} \tag{2.6}$$
$$R_{32,41} = R_{23,14} \tag{2.7}$$
$$R_{43,12} = R_{34,21} \tag{2.8}$$
$$R_{14,23} = R_{41,32} \tag{2.9}$$

and for simmetry

$$R_{21,34} + R_{12,43} = R_{43,12} + R_{34,21} \tag{2.10}$$
$$R_{32,41} + R_{23,14} = R_{14,23} + R_{41,32} \tag{2.11}$$

All measurements have been done with a four wire configuration. Current intensity it was supplied by a Keithley 172 multimeter with 3 μA resolution and a Agilent 34970A sistem has been used for voltage measurements with a 10 nV resolution. For change among different configurations it an analogical commutator was used. All voltage measurements has been acquired for 10 seconds and averaged to reduce noise error. Van der Pauw equation is then solved numerically with the Newton-Raphson algoritm [44] by MATLAB. Thickness d is measured by a Scanning Electron Microscope and resistivity is then calculated by equation 2.3. Typical current values used for electrical measurements go from 1 μA for low conductive films to 10 mA for more compact films.

2.4.2 Mobility and carrier density measurements

A TCO can be modeled with Drude model regarding charge carriers and so this can be used for classical description of Hall effect, based on Lorentz force [14]: a charge moving in a magnetic field $\vec{B}$ with a velocity $\vec{v}$ feels a force $\vec{F}_L$, named Lorentz force, equal to $\vec{F}_L = q\vec{v} \times \vec{B}$ where q is electron charge. So, in a material crossed by a current I, surrounded by a magnetic

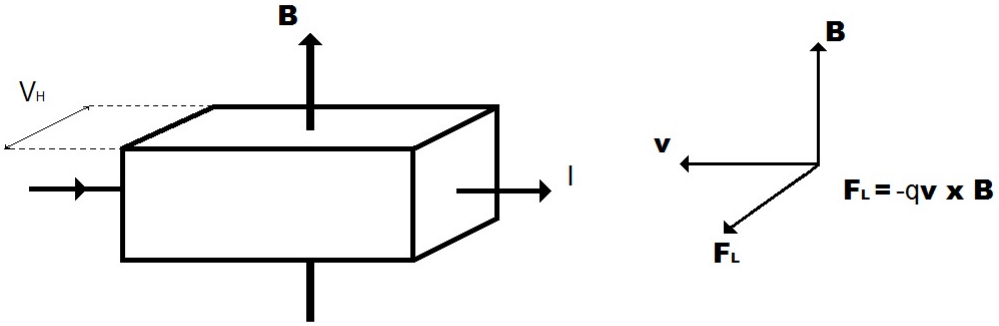

Figure 2.4: Scheme of Hall effect and Lorentz force

field ortogonal to the current direction, an electric potential difference V_H is established, due to Lorentz force on charge carriers, perpendicular both to electric current and to magnetic field. This concept is shown in figure 2.4. It can be demonstrated that, defining τ as electron relaxation time after a fast transitory depending on τ, at regime:

$$V_H = \frac{IB}{end} \tag{2.12}$$

where n is free carriers density and d is film thickness. So, injecting a known current and using a known magnetic field, measured V_H depends only on carrier density:

$$n = \frac{IB}{edV_H} \tag{2.13}$$

We can then evaluate [10]

$$\mu = \frac{1}{en\rho} \tag{2.14}$$

where ρ is resistivity calculated before.

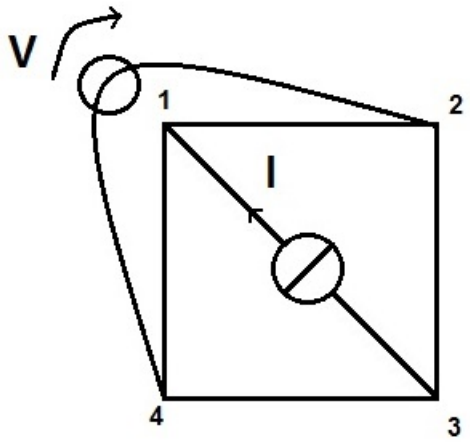

Figure 2.5: Configuration for Hall effect measurements

The same apparatus for resistivity measurements has been used for Hall effect measurements using cross configurations like one in figure 2.5. The current is injected along one diagonal and the Hall voltage is measured along the other one. All configurations have been used changing current direction. In order to eliminate any uneveness and offset in the magnetic field, each mesurement has been done two times with $\vec{B}$ first oriented along positive z and then along negative z. Finally, averaging on different data acquisitions, noise can be eliminated.

2.5 Optical measurements

Transparence, scattering and absorbance measurements have been performed with a UV-vis-NIR PerkinElmer 1050 spectrophotometer. The light source of the spectrophotometer is an alogen deuterium-tungsten lamp an there are two monochromators. They are a holographic grid with 1440 line/mm for ultraviolet and visible and 360 line/mm for infrared. The sistem has

two different detectors, one for high energy and the other for the infrared spectral region. Moreover, an integrating sphere has been used due to high diffusivity of samples deposited at high oxygen pressure. Its role is to collect

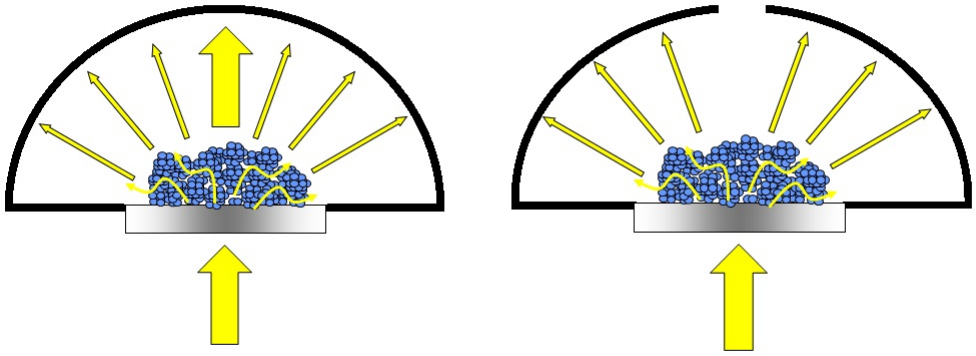

Figure 2.6: Experimental configuration for integrating sphere: on the left scheme for overall transmittance, on the right scheme for scattered transmittance

the transmitted radiation that has been scattered on all solid angle and not only the fraction that has not been deflected. This sphere has two apertures in front of each other. In one, masked with a metallic lamina with a 3 mm diameter circolar hole so as in this range the thickness of the film is almost constant, the light enters in to the sphere. The second aperture has a removable shutter. When removed, the no deflected radiation can exit from the sphere without incides on the photorevelator. So, it is possible to separate the no scattered fraction of light from the scattered one through two different acquisition, one for scattered transmittance and one for overall transmittance. As seen before, the ratio between this two quantities is the haze factor. This concept is shown in figure 2.6.
All spectra were measured with light beam incident on glass substrate first so that it's easy to correct air/glass and substrate interface effects with reference spectrum of bare glass subtracting it to the total spectrum.

2.6 Annealing

On each deposition batch annealing processes have been made. They have been performed with a homemade oven in two different atmosphere. Some samples have been annealed in high vacuum ($p \approx 3 \cdot 10^{-5}$ Pa), others in Argon atmosphere at a slight overpressure (of about 30-50 mbar over air pressure) to prevent oxygen entry in the chamber. In the second case first of all vacuum was reached, then three subsequent gas injection were done to purify the chamber. When the desired atmosphere was ready, a rate of temperature was send into the chamber by a tungsten resistive heater. In this way the temperature, controlled by a termocouple, increased with a rate of $\approx$ 40 °C/min until 500 °C and maintained for one hour. Finally, bias has been turned off with a consequent decrease of temperature. In Figure 2.7 temperature profile is shown. It has been verified by Scanning Electron Microscope that this annealing procedure do not induces relevant morphological variation but only structural.

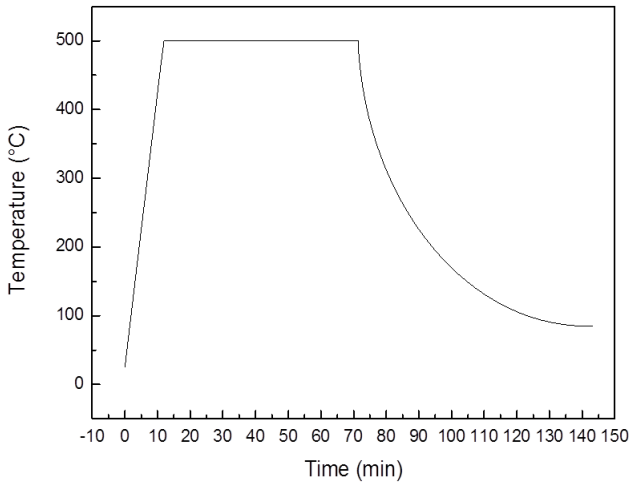

Figure 2.7: Temperature profile used for annealing procedure.

Chapter 3

Experimental results on as deposited samples

In this chapter experimental results are shown and discussed. First of all, two different sample series have been deposited. For both four different batches were deposited, each one with peculiar oxygen pressure, precisely 0,1, 2, 5, 10, 50 and 100 Pa. For every batch one sample was annealed in hgih vacuum and another one in argon pressure. On the first series electrical and optical analysis have been performed in addition to Scanning Electron Microscope (SEM) acquisitions. Thicker second series have been deposited only at 0,1, 2, 10 and 100 Pa pressure to study structural properties. On these films SEM, structural analysis (Raman and X-Ray Diffraction) and electrical measurements have been performed. Thicker films have better Raman and XRD signals. Before deposit compact films an ion gun cleaning was done to prevent delamination typical of these films. Deposition time is 35 minutes for the first series, 90 minutes for 0,1 Pa of second series and 60 minutes for the others samples. Thickness are in Table 3.1. In the end of this thesis work also annealing in argon-hydrogen (at 3%) atmosphere was done. Electrical results on it are in the last section of this chapter.
In this chapter morphological, structural, electrical and optical analysis before annealing are presented. In the first paragraph morphological and structural properties are shown, then last sections are dedicated to functional

properties.

3.1 Morphological and structural properties

In this section fundamental results about morphological and structural characterization are presented and discussed according to Scanning Electron Microscope, X-Ray Diffractor and Raman scattering characterization.
All samples have been deposited with Pulsed Laser Deposition at room temperature with constant distance between target and substrate, laser fluence (1 Jcm^{-2}) and type of gas used in the chamber (O_2). The main parameter changed to control morphology is the oxygen pressure from one sample to another. As described in section 2.1, pressure has a critical role for determining resultant film structure. Modifying it also kinetical energy of ablated species varies and can lead to a cluster formation in the plasma plume. As

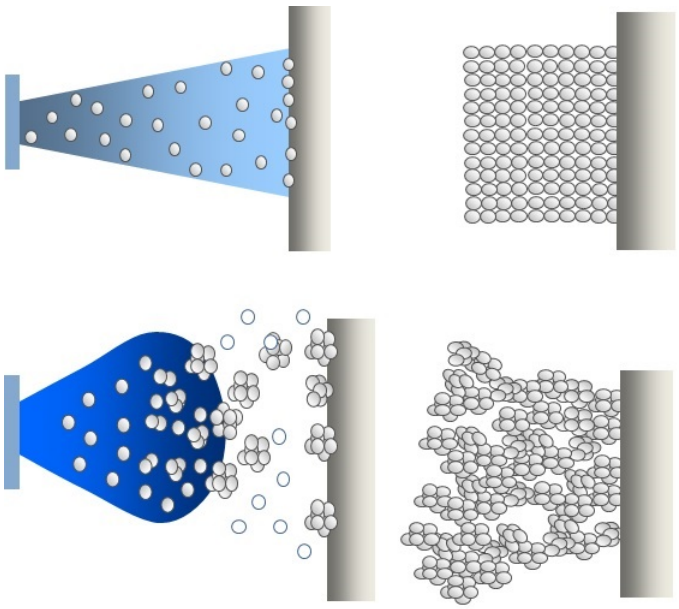

Figure 3.1: Schematic explanation of structure dependence on oxygen pressure. Top:low pressure; bottom:high pressure.

discussed in Section 2.1, low pressure causes a smaller number of collision between ablated species before they reach the substrates. So film growth is

substantially atom by atom and they impact with high surface mobility. In this way atoms can rearrange on the surface creating more compact crystalline grains (Figure 3.1 top).
When increasing oxygen pressure in deposition chamber the probability to have collision between ablated species increases. So nucleations of cluster in the plasma plume take place. They arrive to the substrates with less kinetical energy and low surface mobility. In this case growth is essentially a low energy clusters assembling leading to nanoporous films (Figure 3.1 bottom).

3.1.1 Scanning Electron Microscopy

Cross section images acquired with Scanning Electron Microscope are presented in Figure 3.2. It is evident that changing deposition pressure strongly

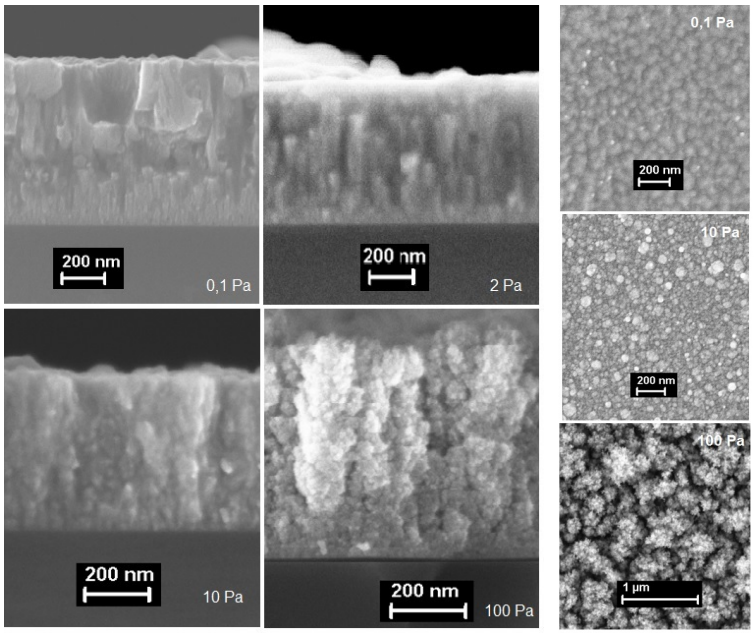

Figure 3.2: Sem images of as-deposited samples. In the right corner there is deposition pressure. On the left there are cross-section, on the right images from top

modifies morphology. For lower pressure (0,1 Pa and 2 Pa) films have a coloumnar preferential direction of growth and are more compact. Moving to pressure of 10 Pa the film is more disordered until at 100 Pa where the

Table 3.1: Average film thickness for the two series and different pressure

Pressure (Pa)	First series (nm)	Second series (nm)
0,1	320	780
2	260	655
5	260	—
10	265	420
50	300	—
100	585	>1000

structure becomes porous and tree-like. Also images from top of the films have been acquired (Figure 3.1 right). They reflect the cross-section images behaviour.
With SEM an evaluation of film thickness was obtained and results are summarized in Table 3.1. Second series samples are characterized by a higher thickness that permit a clear XRD and Raman analysis. All first series samples have been deposited with the same deposition time. It is easy to see that thickness of 100 Pa sample is roughly double than the others. This is due to deposition by cluster that leads to a more porous, less dense and consequently thicker structure.

3.1.2 X-Ray Diffraction analysis

With X-Ray Diffraction cristalline structure of films can be explored. As seen in section 1.3, an XRD spectrum presents some peaks corresponding to crystalline planes (Bragg's law). Analyzing them informations on mean grain domains size and reticular parameter can be calculated through Sherrer's formula, providing information of films cristallinity. In Figure 3.3 relative intensity of ZnO powders is shown [45].
At room pressure and temperature zinc oxide crystallizes in the wurtzite structure, a hexagonal lattice characterized by two interconnecting sublattices of Zn^{2+} and O^{2-} ions. Each Zinc ion is surrounded by a tetrahedron

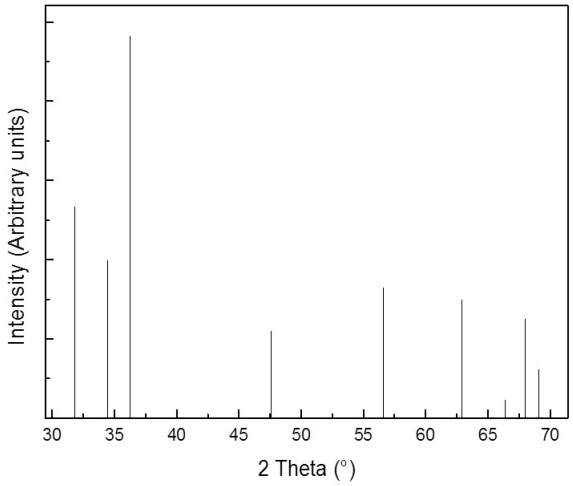

Figure 3.3: Relative intensity of peaks of zinc oxide powders [45].

of oxygen ions and viceversa. In Figure 3.4 X-Ray Diffraction spectra for different deposition pressure are shown. Qualitatively, all films have a well

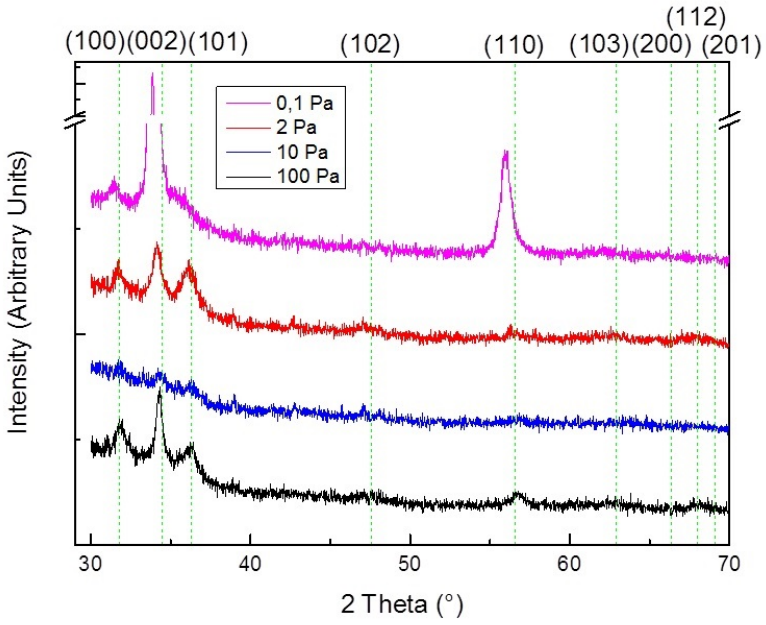

Figure 3.4: XRD spectra for different pressure. Dashed lines indicate reference peaks position for cristalline zinc oxide [45].

defined peak in position between 33.9° and 34.33°. This reflex is significant of the family of basal planes (002) of wurzitic structure resulting in a preferential growth direction. Relative intensity of this peak for film deposited at 10 Pa pressure is lower and this is because it is a thinner film (see Table 3.1) that leads to a worse signal. Also 2 Pa and 100 Pa presents a less intense (002) peak with a simultaneous increase of (100) and (101) reflexes resulting in a more disordered structure. Furthermore, increasing deposition pressure peaks position shifts to higher reflection angle approaching those of zinc oxide position. Also others ZnO peaks appears in XRD spectrum and in particular (110) reflex. However, this peak is less intense than (002) that remains the dominant one. So, film deposited at 0,1 Pa oxygen pressure shows a preferential columnar growth (002) as seen also with SEM. Increasing deposition pressure there is probably formation of nanograins oriented in other different direction but vertical ones remains dominant.
Using Bragg's law and Sherrer's formula data in Figure 3.5 were calculated. Lattice parameter shows a decreasing behavior with a plateau for high pressure with a value of about 5,22 Å, close to equilibrium zinc oxide value of 5,2 Å. This is in agreement with literature [46]. As a matter of fact at low pressure there is a strong atomic structural disorder due to oxygen vacancies. They induce several aluminum and zinc atom to place in interstitial position creating a non stoichiometric structure and generating enlargements in elementar cell. In addition also residual stress can dilate cell in c direction. So, lattice parameter results larger than that of equilibrium for a wurtzitic structure. Increasing oxygen pressure saturation of anionic vacancies leads to a stoichiometry similar to that of zinc oxide and it enhance the entrance of zinc and aluminum ions in substitutional position reducing vertical dimension of elementar cell.
Furthermore, some aluminum ions remain in interstitial position also at high pressure. So, lattice parameter values lower than that of zinc oxide are not reached. As a matter of fact Al^{3+} has an atomic radius lower than Zn^{2+} ones. This is due to the fact that the deposition was done at room temperature. As a matter of fact it has been studied that increasing deposition temperature entrance in substitutional position is favoured with c parameter that assumes

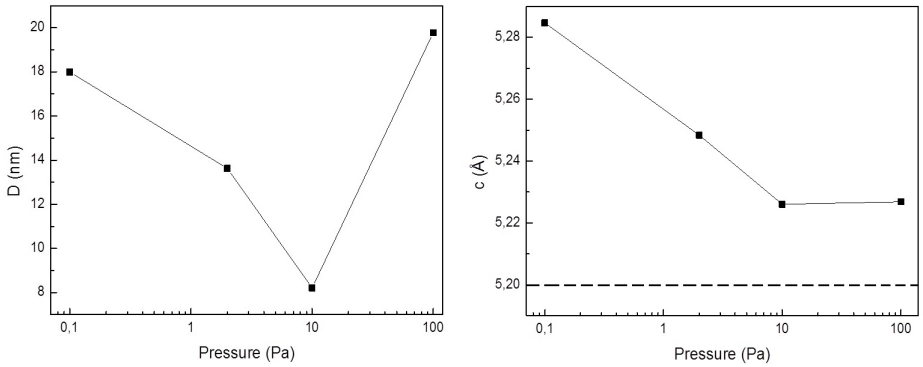

Figure 3.5: Mean domain size on the left and lattice parameter on the right.Dashed line is lattice parameter of crystalline zinc oxide [45]

values lower than wurtzitic ones of powder of zinc oxide [46].
Mean domain size decreases for compact films with increasing pressure with a maximum for 0,1 Pa. The porous film at 100 Pa instead has a D parameter similar to that of 0,1 Pa. Mean cristalline domain size has a behaviour different from literature [36] but an important result is that for 100 Pa. At low pressure D reduces with increasing oxygen in the deposition room. As a matter of fact species are less energetic with a consequent lower surface mobility. For higher pressure this is no longer valid with domains as wide as those of 0,1 Pa.

3.1.3 Raman analysis

State of the art

Raman Spectroscopy is a powerful non-destructive characterization technique to study structural properties, phonons and their interaction with carriers. Zinc oxide crystallizes in the wurtzite structure with a strong uniaxial bond polarity and presents a considerable number of optical phonons at $\vec{q} = 0$, classified according to their symmetry with respect to c-axis. The strong polar character of some modes makes them strongly infrared active and highly resonant near the band edge.

Table 3.2: Frequencies of Raman active modes of wurtzitic bulk zinc oxide

Simmetry	Raman shift (cm^{-1})
A_1-TO	378 ÷ 380
E_1-TO	409 ÷ 413
A_1-LO	574 ÷ 579
E_1-LO	583 ÷ 591
E_2-low	99 ÷ 101
E_2-high	437 ÷ 438

Wurtzitic structure gives rise to polar C_{6v} symmetry along the hexagonal vertical axis c. There are four atoms in the hexagonal unit cell leading to 12 phonon branches, 9 optical and 3 acoustic, classified according to the following irreducible representations:

$$\Gamma = 2A_1 + 2B_1 + 2E_1 + 2E_2 \tag{3.1}$$

Actually, simmetry permits only 6 Raman active modes reported in Table 3.2 [11][47][48].

Qualitatively, E_2 mode at high frequency and E_2 mode at low frequency are associated repectively to vibration of anionic sublattice (formed by oxygen ions O^{2-}) and cationic sublattice (made by zinc ions Zn^{2+}) within the wurtzitic structure. These two peaks are significantly far from each other because the two species have different molecular weight. A_1 and E_1 modes instead are splitted in two components, one transversal (TO) and the other longitudinal (LO) due to ionic bond that generates an intense coulombian field.

Moving from bulk zinc oxide to films it was find that all vibrational modes maintain the same frequencies except for E_1-LO mode that presents a red shift of about 5 cm^{-1} [48] [49]. This effect has been attributed to a reduction of bond strength between lattice ionic couples, with a consequent lower intensity of coulombian field, due to formation of oxygen vacancies, more probable in case of films [11] [48].

Raman spectroscopy is not widely used to study aluminum-doped zinc oxide. This is due to the fact that informations given by this technique are indirect and not univocally linked to functional properties (which could be interesting at industrial level). Furthermore,wavelenghts resonance phenomena that

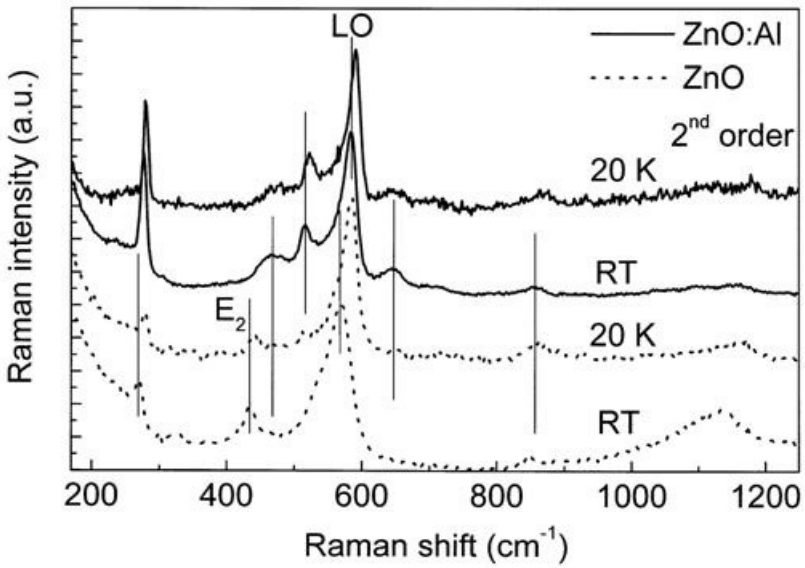

Figure 3.6: AZO and ZnO Raman spectra deposited on aluminum substrates with magnetron sputtering radiofrequency [49]

promotes electrons to an excited state may occur, modyfing the intensity of some Raman modes and making difficult spectra interpretation. Finally, at high oxygen vacancies there is closing of the optical gap with consequent strongly fluorescence phenomena.

A classical AZO Raman spectrum, in Figure 3.6 [49], has an asymmetric band between 550 and 580 cm^{-1} related to A_1-LO and E_1-LO modes. The band at 437 cm^{-1}, typical of ZnO powders, disappears and there is low frequency band up to 300 cm^{-1} linked to E_2-low band. A first interpretation of these spectra is related to oxygen in the film. As a matter of fact, films are substoichiometric in oxygen. So relative intensity between E_2-high band, related to vibration of anionic sublattice,and E_2-low, due to zinc sublattice, changes with respect to zinc oxide spectrum. Band between 550 cm^{-1} and 580 cm^{-1} and E_2-low band are also evidence of structural disorder due to

oxygen vacancies in the lattice.

Raman analysis

Results obtained in this work are in Figure 3.7. The two graphs were obtained one with laser with excitation energy of 532 nm (green), the other with 457 nm (blue). In this second case energy is near to the optical gap and there are some effects of quasi-resonance, due to absorption by the electrons, that increase intensity of some peaks but make spectra more difficult to interpret. Furthermore, instrumentation used for Raman spectroscopy with wavelength of 457 nm do not allow to see peak at 99 cm^{-1}. 10 Pa has a less intense spectrum because it is thinner (420 nm, see Table 3.1) but also some delamination effects may have occurred.

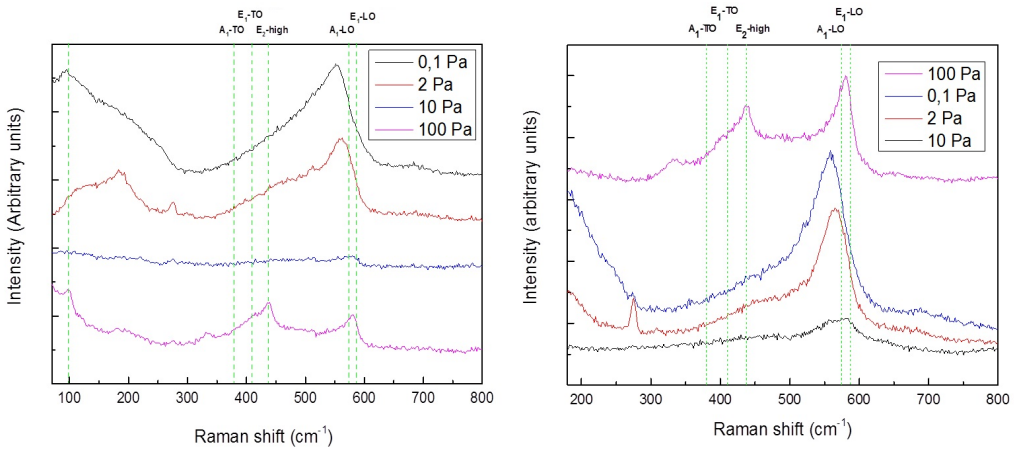

Figure 3.7: Raman spectra for films deposited at different pressure. On the left data achieved with excitation wavelength of 532 nm, on the right 457 nm.

The first thing that can be seen is that increasing deposition pressure, spectra becomes similar to zinc oxide ones. This is due to the fact that at high pressure structure formed are more stoichiometric than that of films deposited at low pressure. Furthermore, at low pressure there are no peaks but bands. This is caused by stoichiometric disorder and grain boundaries that enlarge it. At 99 cm^{-1} peak, linked to the zinc ions sublattice, is already present at low deposition pressure. This could be an indication about the formation

of these structures. It is like that first of all Zn^{2+} sublattice forms at every deposition pressure but only at high pressure oxygen ions sublattice creates. This is also an explanation of substoichiometry in oxygen. So, differently from XRD analysis, structures with more oxygen vacancies present a more disordered spectra (bands). This could be due to a different sensibility of these instruments. XRD gives information about crystalline planes. Instead Raman spectroscopy is sensible to local disorder. Finally, in 2 Pa sample spectrum, a peak at 275 cm^{-1} appears, due to an anomalous mode. This is difficult to interpret. It appears if sample is conductive so it seems related to free charge carriers. This effect will be commented again in Chapter 4 dedicated to annealed samples.

3.2 Functional properties

After structural characterization also functional properties have been studied. Electrical and optical measurements have been performed using instrumentation and methods presented in Chapter 2.

3.2.1 Electrical measurements

A very important characteristic of a transparent conductive oxide is its electrical conductivity. As seen in section 1.1.1 it is

$$\sigma_0 = ne\mu \tag{3.2}$$

So, to increase it carrier density and mobility must be improved. But a high value of n deteriorates optical properties of the film (infrared absorption at plasma frequency) and makes more probable electron-electron scattering. So a fundamental parameter is μ.
In Figure 3.8 a plot of resistivity versus deposition pressure obtained for samples of this thesis work is shown. It has been calculated solving nu-

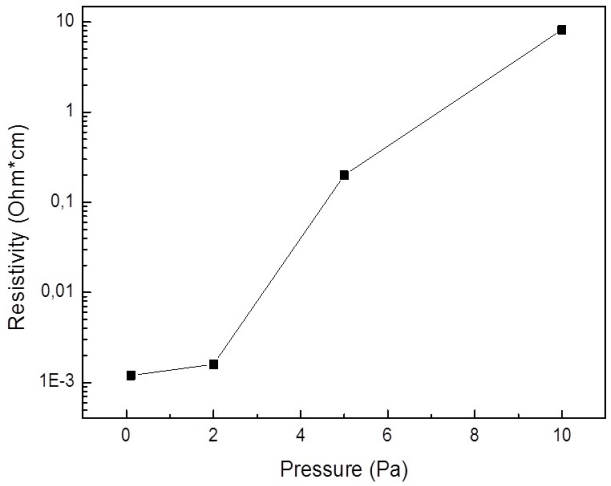

Figure 3.8: Resistivity versus deposition pressure for as deposited samples.

merically (with MATLAB) Van der Pauw's equation (see Section 2.1) using Newton-Rapson's algorithm [50]. There is a minimum of 1,20 x 10^{-3} Ω cm in corrispondence of 0,1 Pa very similar to the value of 2 Pa sample of 1,60 x 10^{-3} Ω cm. Increasing deposition pressure also resistivity increases until at 50 and 100 Pa that results non measurable (this means that they have a resistivity higher than 100 Ω cm, limitation of the instrument).
In Figure 3.9 carrier density and mobility are shown. Carrier density as an optimal value for films deposited at 0,1 and 2 Pa oxygen pressure. Increasing

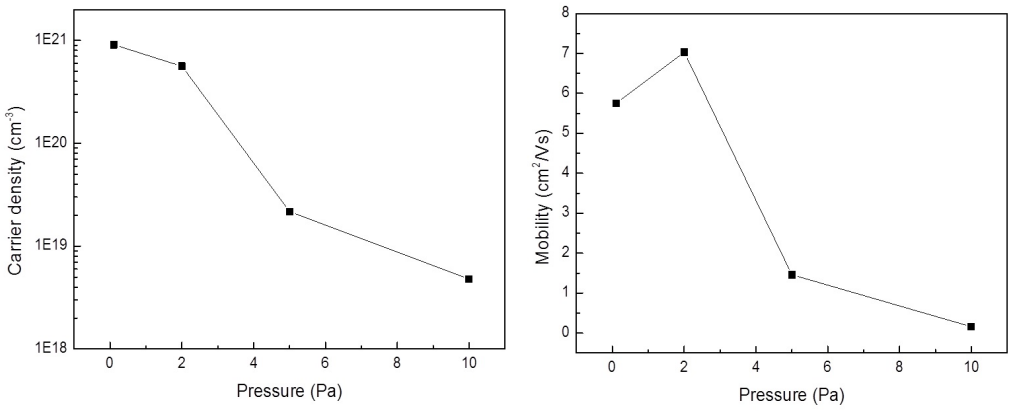

Figure 3.9: Free carrier density (left) and Hall mobility (right) versus deposition pressure for different samples

this deposition pressure carrier density decreases even of two orders of magnitude. On the contrary mobility presents a maximum for 2 Pa case while for film deposited at pressure of 0,1 Pa it is slightly lower. For higher pressure, instead, it significantly decreases. At low pressure high value of n is due to their substoichiometry in oxygen (developed during deposition process) that make them rich in anionic vacancies. At higher pressure the curve undergoes a fall clearly because of reconstruction of zinc oxide stoichiometry.
Looking at mobility, at 0,1 Pa it is lower than that at 2 Pa because first one is full of anionic vacancies significantly enhancing the probability of electron-electron scattering and promotes oxygen segregation at grain boundaries where scattering events are more frequent. These effects decrease mobil-

ity even if film deposited at 0,1 Pa is more crystalline as found with XRD analysis (see Section 3.1.2). At 10 Pa instead film is less crystalline and less compact increasing scattering at grain boundaries with a consequent reduction of μ (mean grain domain size is lower as shown in Figure 3.4). Deposition pressure of 2 Pa represents the optimal compromise between these two situation (stoichiometry and cristallinity) showing a maximum for this value but not for resistivity, contrary to literature samples [24] [36] (see Section 1.3.2). From this data this hypotesis can be done:

- Films deposited at low pressure have a greater concentration of oxygen vacancies than those deposited at higher pressure. This provides a larger number of carriers. As a matter of fact an anionic vacancy behaves as a two electrons donor.
- After 2 Pa resistivity increases a lot till unmeasurable values for samples deposited at 50 and 100 Pa oxygen pressure. This is due to the lower number of oxygen vacancies together with a no connected structure.
- Films deposited at low pressure are rich in reticular defects due to oxygen substoichiometry. This has a consequence on electron-electron scattering and on oxygen at grain boundaries affecting mobility (see Section 1.1.1).

It is important to underline that Drude's model used to describe Hall effect is a free electron model. For more complicated structures like those in this thesis work, particularly for low conductive samples, reliability of Drude's model begin to drop with a greater uncertainty.
Comparison between the two series confirm electrical measurements. As a matter of fact, for film thicker than 200 nm thickness slightly influences electrical properties [51].

3.2.2 Optical measurements

In Figure 3.10 the transmittance spectra of deposited samples are shown. Since compact and porous films have different behavior, they are plotted

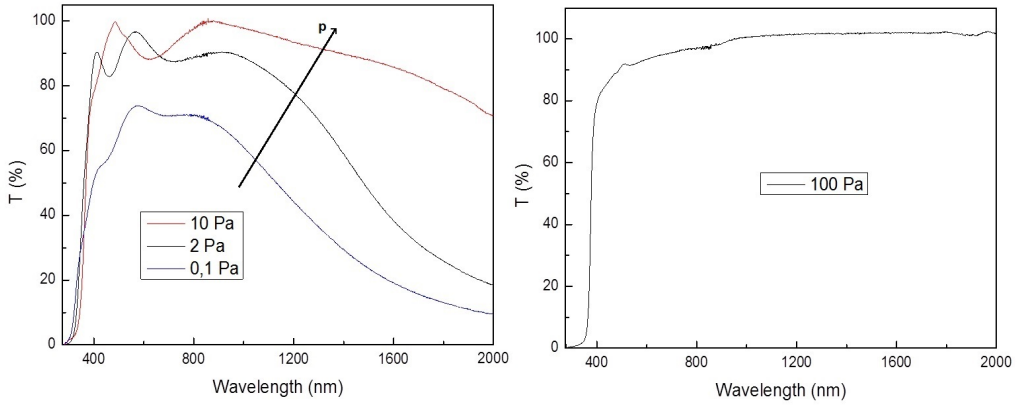

Figure 3.10: Transmittance spectra of compact (left) and porous (right) films. Transmittance spectra of porous sample have been done for film deposited at a slight high pressure, comparable with sample deposited at 100 Pa.

separated. On the left spectra of conductive films are shown. They present some typical characteristics common to all TCOs (see Section 1.1.2). Below wavelength related to optical gap (see Section 1.3.3) all radiation is absorbed. As a matter of fact it has enough energy to promote electrons to conduction band. Increasing wavelength also degree of transparency rapidly increases and presents typical interference fringes whose profile substantially depends on thickness, roughness and refraction index of the film. Decreasing energy of incident photons, region in which carriers absorb electromagnetic radiation through collective oscillations (plasmons) is reached. Here transmittance fall down above 800 nm. This effect confirms the great number of charge carriers with a behavior similar to that of free electrons gas well described by Drude model.

On the right of Figure 3.10 there is transmittance spectrum of porous film (deposited at 100 Pa oxygen pressure). It is really different from those of compact films. First of all rising edge of transmittance profile in corrispon-

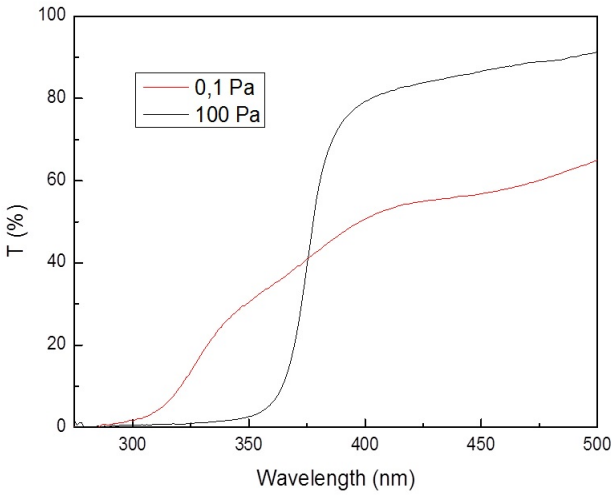

Figure 3.11: Comparison of behavior about optical gap between compact and porous film

dence of optical gap is significantly steeper and narrower. This fact can be seen in Figure 3.11 and it is a consequence of the lower concentration of interband defects. In visible range (see Figure 3.10) there is no oscillation profile. This is due to a strong morphological disorder that does not permit optical coherent phenomena. Furthermore, surface of porous films is so irregular that prevents possible coherent phenomena at the interface with air. Finally, in the infrared there is no absorption. This is due to less carrier for this kind of structure.

In Figure 3.12 mean transparency for different pressure is shown. It is evident that increasing deposition pressure also transparency increases with high percentage (near to 95%) for films deposited at 100 Pa. This fact is due to reduction of defect states that can absorb incident photon but also to a less dense structure for films deposited at 100 Pa.

As discussed in Section 1.2 a peculiar characteristic of hierarchical films is their ability to trap and scatter light. This property is well described by a coefficient called haze factor. If T is total transmitted light and S is the

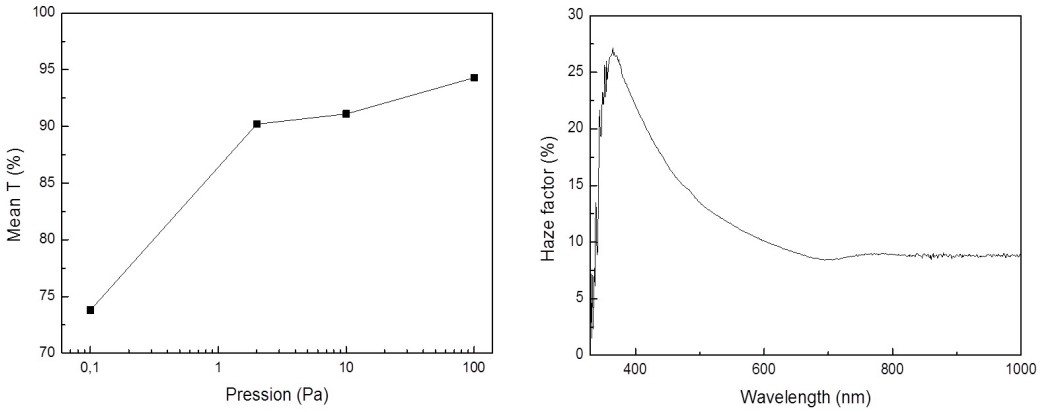

Figure 3.12: Mean transmittance for different pressure (left) and Haze factor for 100 Pa sample (right)

scattered one, haze factor H is in percentage

$$H = \frac{S}{T} \tag{3.3}$$

Figure 3.12 on the right shows haze factor for sample deposited at 100 Pa oxygen pressure. It can be see that in the visible range haze factor is high because of morphology of this kind of film. At deposition pressure of 200 Pa haze factor reaches values near to 100 % [36]. Haze factor has been calculated also for compact film but results are not presented because they are no significant (haze factor is near 5 % along all spectrum). This behavior can be understood looking at SEM images (Figure 3.2). It is evident that a porous film is able to scatter transmitted light in all directions. This is due to arborescent structure visible in SEM image which scatter photons with wavelengths similar to characteristic dimension of nanocluster. This difference in scattering is visible also to the eye. As a matter of fact, compact films look transparent in contrast with porous films that appears white because of their higher diffusivity degree. Haze factor, in addition, is high in the visible range but falls down at higher wavelengths. In this case wavelength of incident light is higher than characteristic dimensions of nanostructures.

3.3 Discussion and conclusion

In this section a brief discussion of the relation between morphology, structure and functional properties is presented. It is evident that compact and porous films have different properties. This is mainly due to crystallinity and carrier density. As seen with X-Ray Diffraction (Section 3.1.2) compact films have a high order of cristallinity with larger grain domain size. In addition, because they were deposited with low oxygen pressure, they are rich of anionic vacancies that results in a carrier density. For these reasons they are very conductive and with good mobility values.

Optimal case in literature [36] has not been reached for these sample. There are two main reasons for this. First of all during this thesis work some components of the laser (second armonic generator and transmittance window) gives some problems influencing fluence of the laser. This has an impact on kinetic energy of ablated species reducing it. So samples show a lower mobility than literature ones (attested on about 20 cm^2/Vs [36][24]). Another reason of this behavior is that the optimal value is for film with thickness of about 1 μm. All of the conductive films are thinner than this value, increasing scattering probability. Despite this difference in optimal value, general behavior is similar to that of literature. Comparing XRD and Raman spectra it can be deduced that crystalline quality of samples deposited at 2 Pa is better but also that of 0,1 Pa is very similar.

Samples with highest mobility have also the largest domain size calculated from XRD analysis. So, mobility is directly related to cristallinity of the film. Difference between 0,1 and 2 Pa deposited samples is due to a number of carriers higher in the case of 0,1 Pa resulting in a greater electron-electron scattering probability but also in more oxygen segregated to grain boundaries. This large density of carrier is verified also by Raman analysis that shows a substoichiometry for compact films corresponding to a great number of oxygen vacancies and, so, electrons. There is a strong reduction of defects increasing deposition pressure. This fact is confirmed also by optical analysis. In fact, at higher pressure steeper rising edge of transparency and a greater mean transparency in visible range was observed. Furthermore, large

carrier density is justified also with strong reduction of transparency in infrared region. This fact is due to absorbance of light by collective oscillation of electrons called plasmons.
Porous films are hierarchically structured as seen with Scanning Electron Microscope. With X-Ray Diffraction analysis they look very crystalline with a mean grain domain size near to that of 0,1 Pa but Raman spectra show that they have also a stoichiometry similar to that of zinc oxide. So, their low conductivity is justified. As a matter of fact, they have a very low carrier density due to their lack of oxygen vacancies. This make these films really resistant to current flow. Porous films shows also a mean transmittance higher than compact films. Clearly, having few free electrons, this structures do not show absorption in infrared region due to plasmonic effect resulting transparent in this range. Besides, they do not present coherent interference fringes typical of compact films. Porous films, that presents also dendritic structures visible at SEM images, have also good light trapping properties measured by haze factor. Compact films do not present these nanostructeres and, in fact, have very low scattering properties.

Chapter 4

Effects of annealing in different atmospheres: experimental results

In this chapter results about samples annealed in different atmosphere are shown and discussed. One sample of every batches have been annealed using procedure explained in Section 2.4. Electrical,optical (Section 4.2), morpholocical (Section 4.1.1) and structural (Section 4.1.2 and 4.1.3) were done on each annealed sample and finally compared and discussed in Section 4.3 and 4.4.

4.1 Morphological and structural properties

First of all, Scanning Electron Microscopy was used to study the morphology of the films and to verify there were no relevant cracks or variation at nano or meso-scale levels on the samples due to annealing. Then structural analysis was done through X-Ray Diffraction and Raman scatterin. The results will be presented first for high vacuum annealing and then for annealing in argon atmosphere.

4.1.1 Scanning Electron Microscopy

SEM images were acquired to see any changes in the structure. The general behavior is common to all different samples. For this reason in Figure 4.1

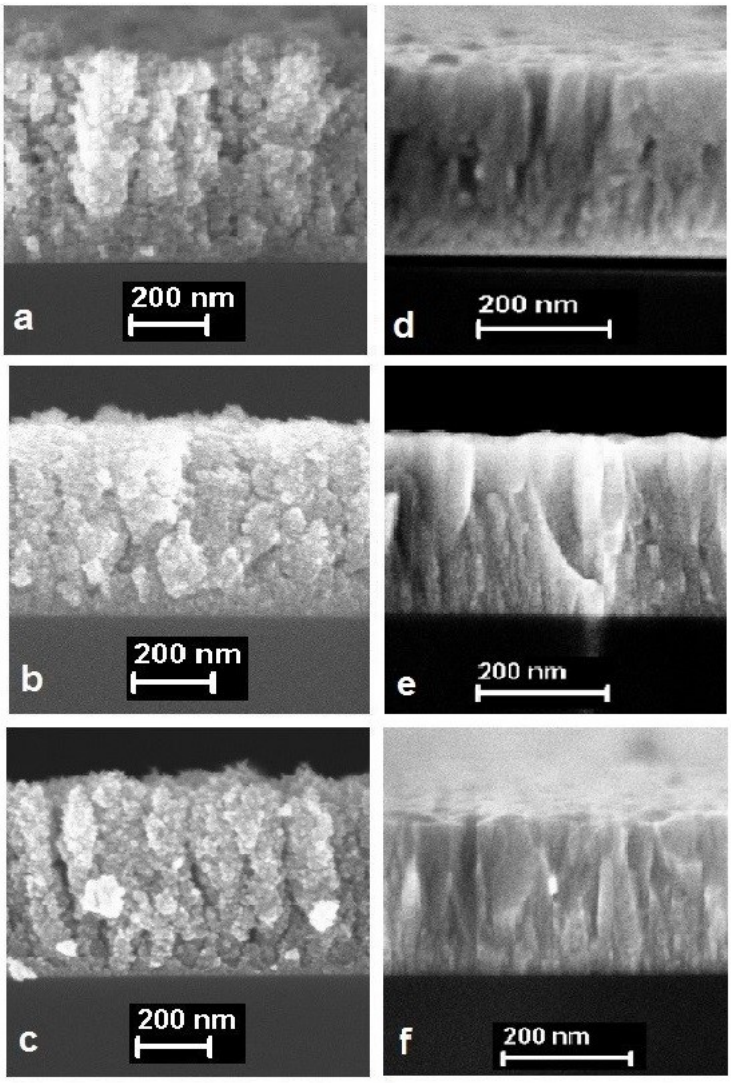

Figure 4.1: SEM images of samples deposited at 0,1 Pa (a,b,c) and 100 Pa (e,d,f) oxygen pressure. Images a and d are of as-deposited samples, b and e vacuum annealed, c and f argon annealed.

only samples deposited at oxygen pressure of 0,1 Pa (compact) and 100 Pa (porous) are shown as representative of compact and nanoporous structures. Looking these images it is clear that:

- Thickness is constant after annealing both for compact and for porous films
- Samples are more interconnected after annealing as if a sintering is occured. This is more evident for samples deposited at 100 Pa oxygen pressure.
- Interconnection seems to be slightly stronger for sample annealed in high vacuum for porous film (Figure 4.1 b) and in argon atmosphere for compact ones (Figure 4.1 f).

SEM images were acquired also to verify if samples present connected cracks on their surface due to the annealing process. Only for the case of sample deposited at 0,1 Pa few isolated cracks of the order of 1 μm (Figure 4.2) appear only for the case of annealing in argon atmosphere. So, they do not affect functional properties of the film. This is probably due to the particular morphology of these structure that prevents cracks formation. As a matter of fact, samples deposited at 0,1 Pa oxygen pressure could be characterized by an elevate stress before annealing.

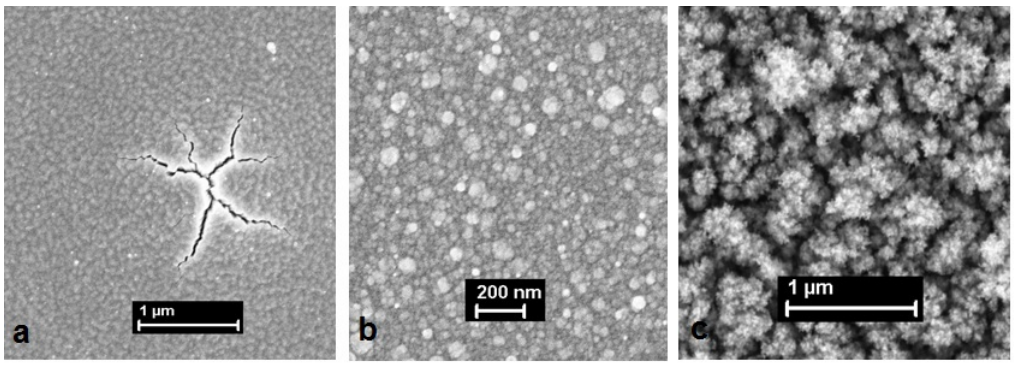

Figure 4.2: SEM images of samples annealed in argon atmosphere. Image a is for deposition pressure of 0,1 Pa, b 10 Pa and c 100Pa.

4.1.2 XRD analysis

XRD analysis after annealing in high vacuum

In Figure 4.3 XRD spectra of samples annealed in high vacuum for different deposition pressure are shown. All films have a well defined (002) peak really

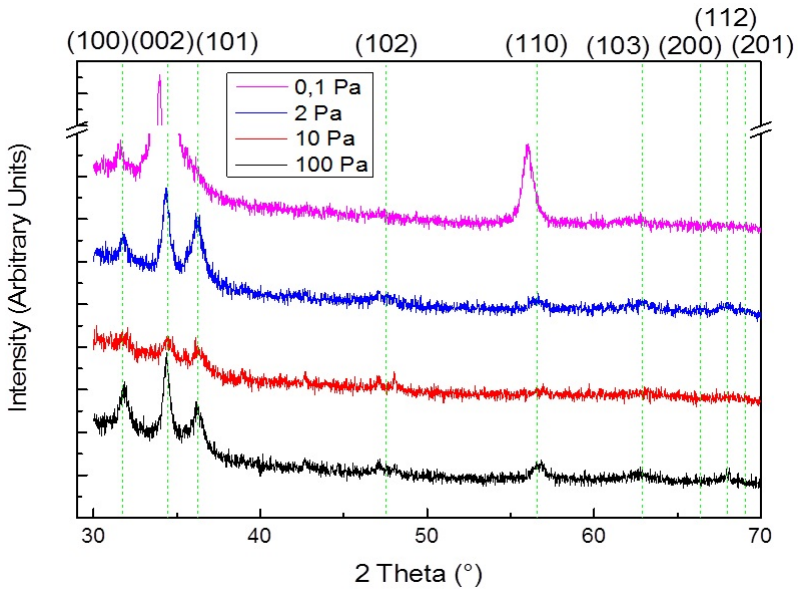

Figure 4.3: XRD spectra for different deposition pressures for samples annealed in vacuum. Dashed lines indicate reference peaks position for crystalline zinc oxide [45]

close to reference zinc oxide (002) line that shows that all films have a vertical preferential orientation growth. Also (110) peak appears for all spectra, especially for 0,1 Pa pressure. The other samples show also (100) (weak for 0,1 Pa case) and (101) peaks. This means that increasing deposition pressure resulting structure are formed by nanograins with different orientation.
As for as deposited samples increasing pressure leads to film with structure similar to that of zinc oxide and also samples deposited at 2 Pa and 10 Pa oxygen pressure have peaks really close to zinc oxide reference with (002) peak that remains the dominant one. Peaks intensities result roughly doubled with respect to as deposited samples and (002) peak for 0,1 Pa pressure case is wider.

In Figure 4.4 mean domain size D and lattice parameter c are shown. Mean

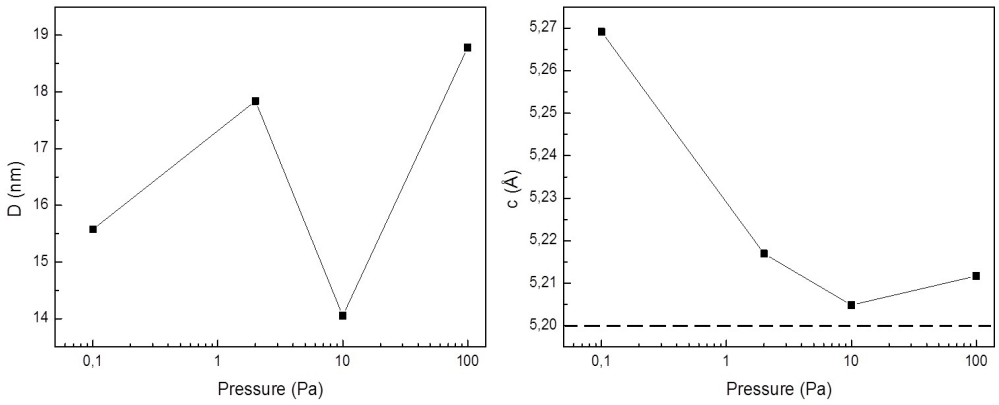

Figure 4.4: Mean domain size for different pressures (left) and reticular parameter (right). Dashed line is reticular parameter of crystalline zinc oxide [45]

domain size has not a linear behavior but is always between 14 and 19 nm. Minimum value is for 10 Pa pressure and maximum for 100 Pa pressure like in the case of as-deposited samples.
Lattice parameter instead shows a decreasing behavior until 10 Pa deposition pressure with a slightly increase for 100 Pa. Also in this case no samples have c values lower than equilibrium zinc oxide value of 5,2 Å. It seems that there is a *plateau* from 2 Pa (variations in lattice parameter are small). This fact could be due to a rearrangement of aluminum and zinc ions during the annealing process that permits to Al^{3+} and Zn^{2+} to be in substitutional position reducing vertical dimension of elementary cell.

XRD analysis after annealing in argon atmosphere

In Figure 4.5 spectra for different deposition pressure for samples annealed in argon atmosphere are shown. In this case all samples except the sample deposited at pressure of 0,1 Pa have (002) peak in the same position of zinc oxide. Intensity is higher than in as-deposited samples but also than vacuum annealed ones (a deeper discussion of this is in Section 4.3). (110) peak is present for all deposition pressures with a relative intensity higher in the case of 100 Pa. Sample deposited at 0,1 Pa shows an intense (non relatively) (110)

peak present in all the others spectra. A relative strong (101) peak appears for 2 Pa, 10 Pa and 100 Pa pressure samples.
Also in this case increasing pressure leads to films with structure similar to that of crystalline zinc oxide but in this case also samples deposited at 2 Pa and 10 Pa oxygen pressure have peaks really close to zinc oxide reference with (002) peak that remains the dominant one. Peaks intensity sre about three times than as-deposited samples.
In Figure 4.6 mean domain size D and lattice parameter c are shown. Graph

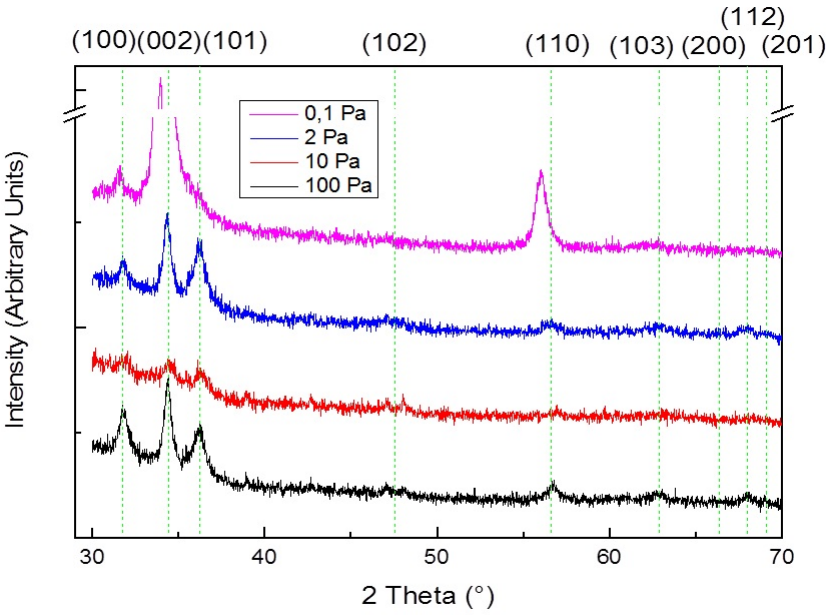

Figure 4.5: XRD spectra for different deposition pressures for samples annealed in argon atmosphere. Dashed lines indicate reference peaks position for crystalline zinc oxide [45]

on the left shows a behavior of D similar to that of as-deposited samples. As a matter of fact mean domain size decreases with increasing pressure until 10 Pa but then increases at 100 Pa deposition pressure.
Also c (vertical parameter of unit cell) has similar behavior. Annealing in argon atmosphere permits a strong rearrangement of aluminum and zinc ions with many of them occupying substitutional position instead of interstitial. Also in this case no samples have c parameter lower than that of crystalline

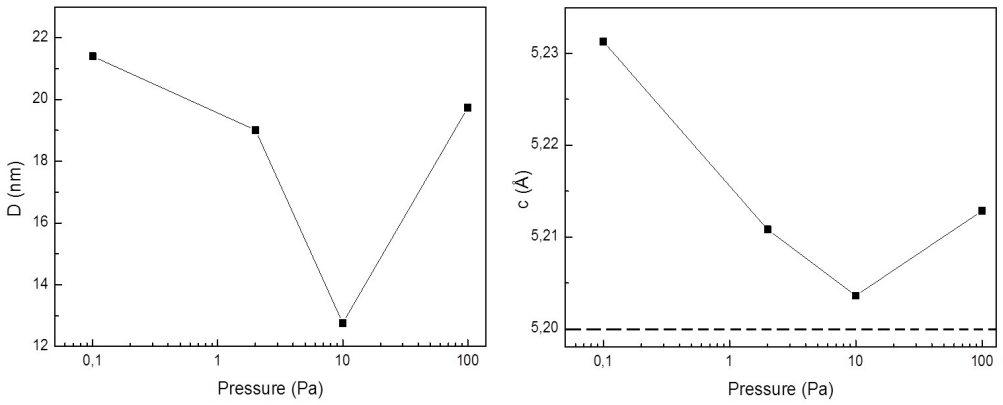

Figure 4.6: Mean domain size for different pressures (left) and reticular parameter (right). Dashed line is reticular parameter of crystalline zinc oxide [45]

zinc oxide, represented in Figure 4.6 (right) with a dashed line.

4.1.3 Raman analysis

Raman analysis after annealing in high vacuum

In Figure 4.7 Raman spectra at different deposition pressure for samples annealed in high vacuum are shown. On left spectra obtained with excitation wavelength at 532 nm are shown, on right at 457 nm in pre-resonance configuration. Spectra with low signal were obtained for sample deposited at pressure of 0,1 Pa so they are not shown. Also in this case when increasing deposition pressure spectra become similar to zinc oxide ones because structures become more stoichiometric with E_2^{high} band, related to oxygen sublattice, that becomes peak. Also in this case peak at 99 cm^{-1} is present, well defined for 100 Pa pressure, related to zinc sublattice. However, spectra of samples deposited at low pressure show bands and wide peaks. This is due to substoichiometry of these structures.
A peak at 275 cm^{-1} (anomalous mode) appears for all deposition pressure. As discussed later (Section 4.2.1), these films are more conductive than as-deposited ones. So, as suggested in Section 3.1.3, this peak could be related to free charge carriers. This relation is phenomenological but seems to be confirmed by experimental data.

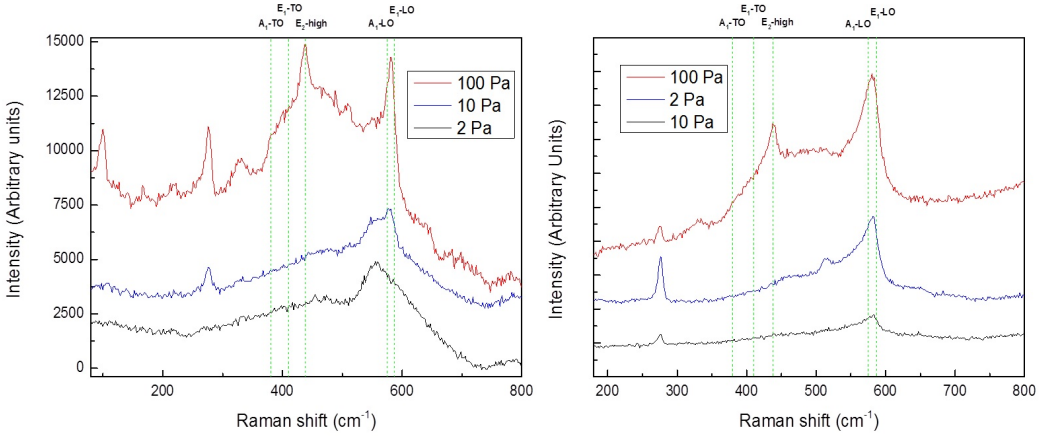

Figure 4.7: Raman spectra of samples for different pressure annealed in high vacuum. On the left data obtained with excitation wavelength at 532 nm, on the right with excitation at 457 nm.

Raman analysis after annealing in argon atmosphere

In Figure 4.8 Raman spectra at different deposition pressure for samples annealed in argon atmosphere are shown. On left spectra obtained with excitation wavelength at 532 nm are shown, on right at 457 nm in pre-resonance configuration. Again, increasing deposition pressure spectra become similar

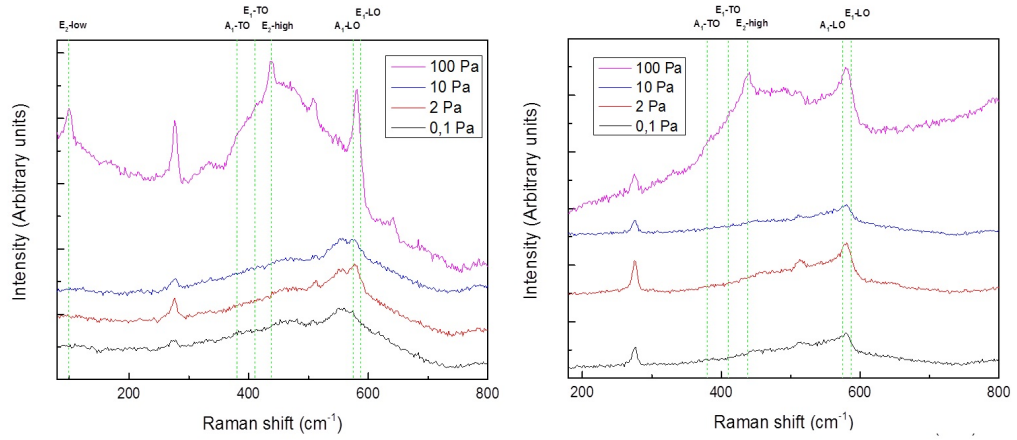

Figure 4.8: Raman spectra of samples for different pressure annealed in argon atmosphere. On the left data obtained with excitation wavelength at 532 nm, on the right with excitation at 457 nm.

to zinc oxide ones because structures become more stoichiometric. Peaks intensity is five times the case of as-deposited samples and doubled compared to spectra of samples annealed in high vacuum. Peaks are better defined for 100 Pa deposition pressure but spectra are still disordered (substoichiometry in oxygen) for low deposition pressure. Also in this case the peak at 99 cm^{-1} is present, well defined for 100 Pa pressure, related to zinc sublattice.
In these spectra the peak at 275 cm^{-1} (anomalous mode) appears strongly at all deposition pressure. As discussed later (Section 4.2.1), these films are more conductive than as-deposited and annealed in vacuum samples. This is another evidence that supports the hypothesis that this peak is related to free charge carriers. For samples annealed in argon anomalous mode is intense for all samples and appears for both excitation wavelengths. A correlation between this peak and conductivity of the films will be shown in Section 4.3 after discussing th functional properties of these films.

4.2 Functional properties

In this chapter electrical and optical properties of annealed films are shown. These measurements were done using the apparatus explained in Chapter 2. Results will be shown together both for samples annealed in high vacuum and for those annealed in argon atmosphere. Comparison with as-deposited samples is in Section 4.3.

4.2.1 Electrical measurements

In Figure 4.9 resistivity for samples annealed in high vacuum and in argon atmosphere is shown. The behavior of the two curves is similar. Optimal

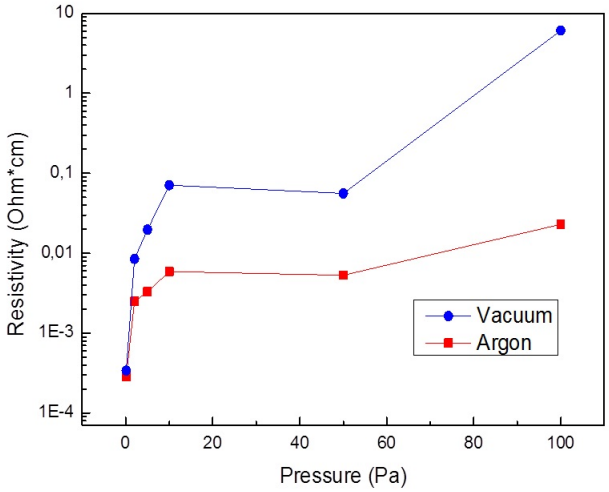

Figure 4.9: Resistivity versus oxygen deposition pressure for annealed samples.

value of about 3x10^{-4} Ωcm is for sample deposited at pressure of 0,1 Pa. Increasing pressure also resistivity increases reaching a *plateau* for pressure higher than 10 Pa. At 100 Pa oxygen pressure resistivity increases for both annealing but slightly for annealing in argon atmosphere. Annealed samples deposited at 50 and 100 Pa pressure resulted to be conductive in contrast to the case of as-deposited samples for wich they resulted non measurable (see Section 3.2.1).

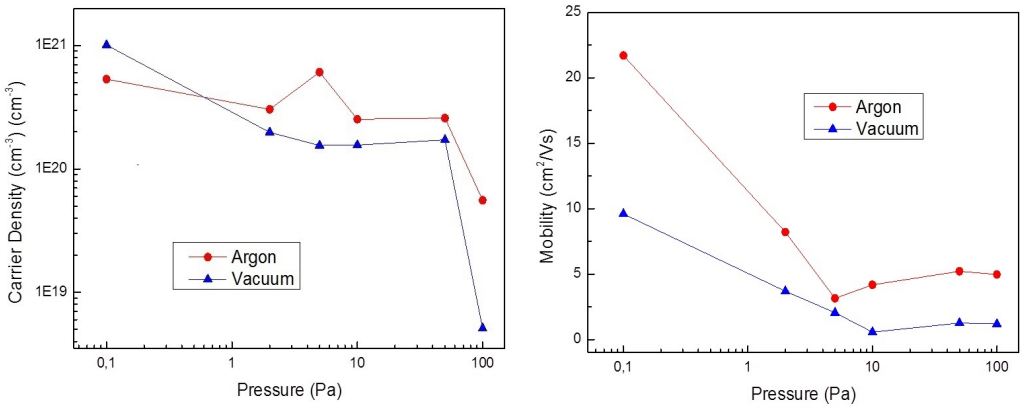

Figure 4.10: Carrier density (left) and mobility (right) versus oxygen deposition pressure for annealed samples.

In Figure 4.10 free carrier density and mobility are shown. Until 50 Pa these two quantities have a similar behavior. Carrier density has an optimal value for sample deposited at pressure of 0,1 Pa of about 10^{21} cm^{-3} for annealing in high vacuum and 9x10^{20} cm^{-3} for argon atmosphere. Actually, for this second case the maximum is at 5 Pa deposition pressure. From 5 Pa pressure in the case of annealing in high vacuum and from 10 Pa for argon annealing there is a *plateau*. Also in this case, samples deposited at 50 and 100 Pa pressure were measurable contrary to as-deposited ones and porous samplesshows a strong reduction in carrier density

Also mobility until 50 Pa presents a similar trend but differs from carrier density for sample deposited at 100 Pa. Maximum is for samples deposited at pressure of 0,1 Pa with mobility values of about 9,6 cm^2/Vs for high vacuum annealing and 21,7 cm^2/Vs for argon annealing. Mobility decreases with increasing pressure reaching a *plateau* from about 5 Pa. Contrary to as-deposited films, 2 Pa pressure is no more the optimal compromise between stoichiometry and crystallinity as said in Section 3.2.1.

Analyzing previous data, best results were obtained for annealing in argon atmosphere both for carrier density and for mobility. This fact explains the resistivity behavior that depends on both parameters (Equation 1.1).

Annealing base pressure dependence of electrical properties

As said in section 2.4, base pressure for both annealing is of about 3x10^{-5} Pa. In preliminary measurements of this work another base pressure had been used of about 10^{-3} Pa. In this section results obtained with these two different starting pressure will be presented to explain the choice made. In Figure 4.11 resistivity versus deposition pressure after annealing in high vacuum and in atmosphere is shown. Improvement starting with lower base pressure is

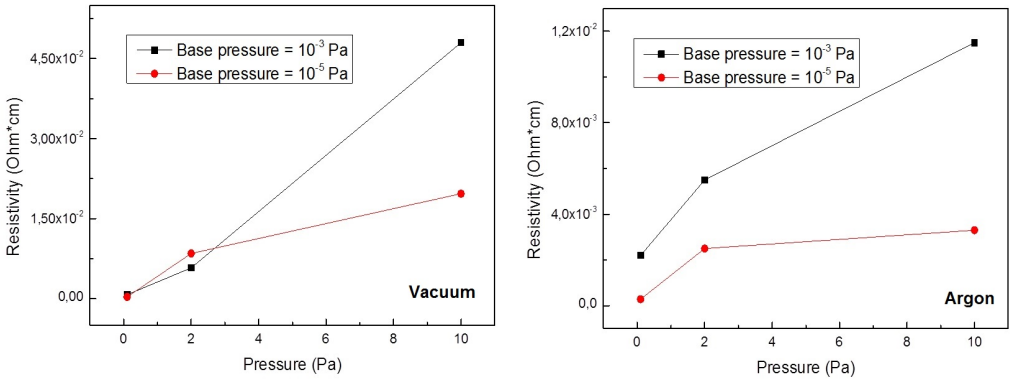

Figure 4.11: Resistivity versus deposition pressure for different base pressure for annealing in high vacuum (left) and in argon atmosphere (right).

evident, especially at high deposition pressure. Samples deposited at 50 and 100 Pa annealed with base pressure of about 10^{-3} Pa is not measurable while for 10^{-5} Pa electrical measurements give good results (see Figure 4.9). For annealing in argon atmosphere the gain is important also at low pressure, increasing with deposition pressure.

Also carrier density and mobility show a significant improvement. The results are plotted in Figure 4.12. Carrier density for samples annealed in high vacuum shows better results for 0,1 Pa and 10 Pa pressure. In the case of 0,1 Pa the improvement is of one order of magnitude. With annealing in argon atmosphere improvement is better starting from pressure of 10^{-5} Pa but lower than for vacuum annealing. On the contrary, mobility shows a decrease after annealing in vacuum atmosphere at lower base pressure but it improves in the case of argon annealing. This fact can be explained assuming

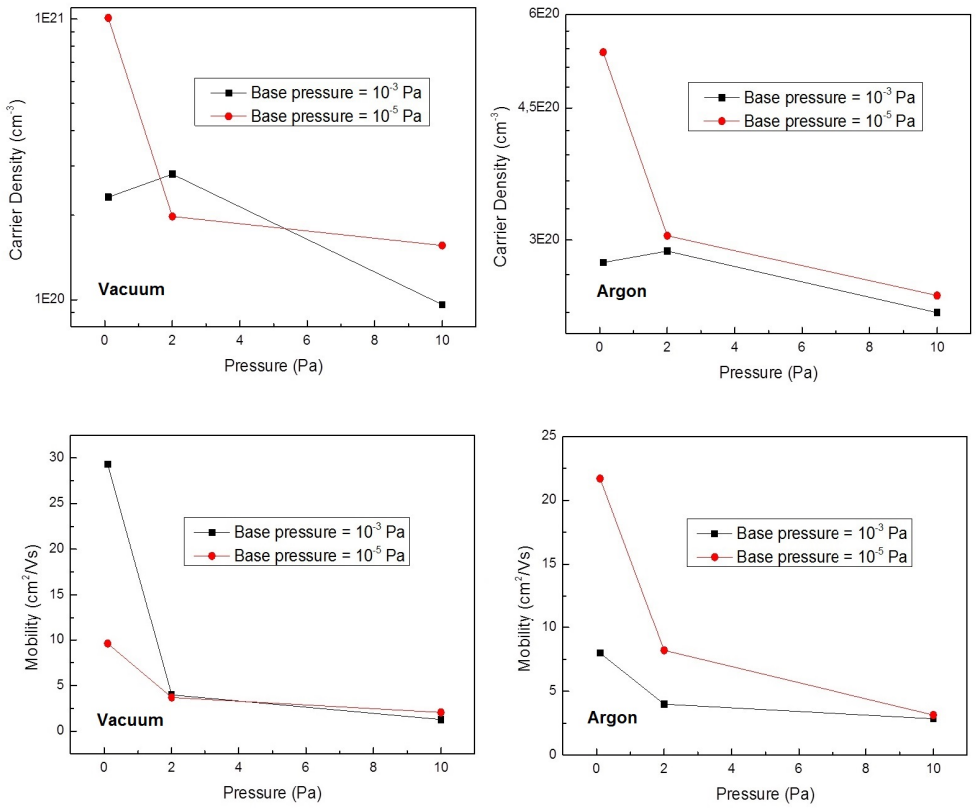

Figure 4.12: Carrier density (top) and mobility(bottom) versus deposition pressure for different base pressure for annealing in high vacuum (left) and in argon atmosphere (right).

that during annealing two different processes can occur. First of all there is a probable moving of interstitial aluminum and zinc ions to substitutional position due to high temperature. The second process is oxygen desorption due to high temperature (500 °C). This oxygen could be both reticular but also at grain boundaries. In the first case substoichiometry changes creating more oxygen vacancies (and consequently free electrons) and chemical disorder. When the oxygen at grain boundaries desorb instead mobility increases as a consequence of reduced trap. So, in the case of annealing in high vacuum (especially for sample deposited at 0,1 Pa pressure) that could results in some air contamination strong increasing in carrier density with lower base pressure probably means that there were a large desorption of reticular oxygen with consequent reduction in mobility. In the case of annealing in argon atmosphere increasing in carrier density is not so strong (and so also oxygen desorption) allowing to have a more ordered structure with higher mobility.

4.2.2 Optical measurements

In figure 4.13 transmittance spectra of samples annealed in high vacuum and in argon atmosphere are shown. Films deposited at 100 Pa pressure present a similar behavior. As in as deposited samples, rising edge of transmittance profile is steep and narrow due to low concentration of interband defects. In visible range there is still no oscillation profile and no absorption in the infrared.

Compact films instead have different behavior. Samples deposited at 2 Pa films are similar with two interference fringes in the visible range, similar rising edge and analogue plasmonic absorbance, with transmittance at 2000 nm of the order of 40 %. In this region instead films deposited at 10 Pa pressure have a quite different behavior, with a stronger absorption due to plasmonic effect for the case of film annealed in argon atmosphere. Profiles for 2 Pa deposition pressure are very different. Sample annealed in high vacuum presents a strong absorption in infrared and a mean transmittance in visible range of about 75 % as shown in Figure 4.14. In the case of argon annealing spectrum is very similar to that of sample deposited at 2 Pa. It

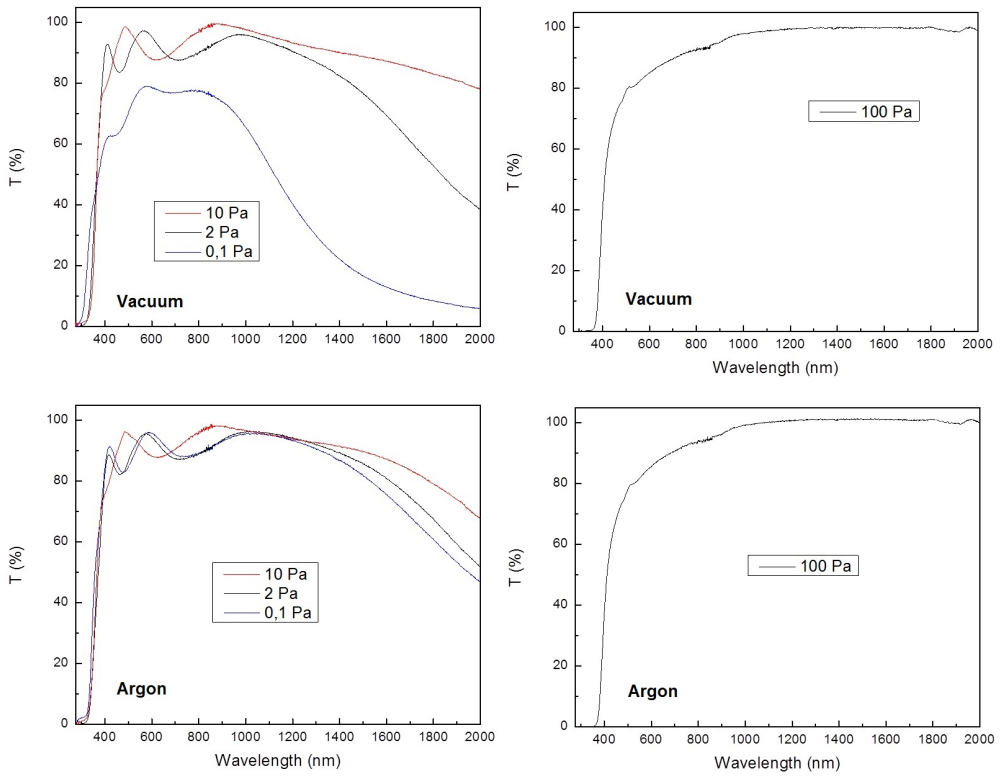

Figure 4.13: Light transmittance of compact (left) and porous (right) films for samples annealed in high vacuum (top) and in argon atmosphere (bottom). Transmittance spectra of porous sample have been done for film deposited at a slight high pressure, comparable with sample deposited at 100 Pa.

has well defined interference fringes, mean transmittance around 90 % and lower absorption in the infrared due to free charge carrier. This is related to different carrier density as shown in Section 4.2.1. Sample deposited at a pressure of 0,1 Pa and annealed in high vacuum have a free charge concentration that is almost one order of magnitude greater to that of films annealed in argon atmosphere. This results in a lower number of oscillating electrons that absorb light.

In Figure 4.14 mean transmittance in visible range versus deposition pressure is shown. For films deposited at 0,1 Pa behavior is different reflecting different transparency profile seen before. The other films show a similar trend, with high transmittance for lower pressure and a fall for 100 Pa. However, these are very transparent in infrared range.

In the same Figure also haze factor of samples deposited at pressure of 100 Pa is shown. Behavior of annealed films is very similar with a higher maximum for samples annealed in argon atmosphere. Also in these case haze factor is high in the visible range but falls down beyond visible range, where wavelength of incident light is higher than characteristic dimensions of nanostructures.

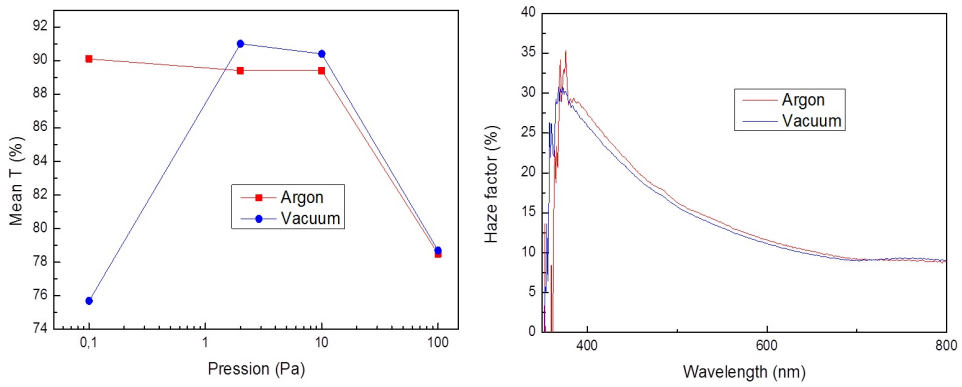

Figure 4.14: Mean transmittance versus deposition pressure on the left and haze factor of sample deposited at 100 Pa on the right for films annealed in high vacuum and in argon atmosphere

4.3 Comparison between as deposited and annealed samples

Before discussing results, a brief comparison between as deposited and annealed samples is presented in this Section. In Paragraph 4.1.1 it has been shown that morphology slightly changes, making structures after annealing more interconnected but maintaining the thickness constant. In next Sections comparison of structural and functional properties will be shown.

4.3.1 Structural properties

X-Ray Diffraction

In Figure 4.15 XRD spectra for different pressure and annealing treatment are shown. Samples deposited at 0,1 Pa pressure shows a strong preferential direction of growth (002) and a relative less intense peak at (110). Annealed films have peaks nearer to reference position of crystalline zinc oxide and also narrower than as-deposited ones, especially after argon annealing. Also sample deposited at 2 Pa shows peaks near zinc oxide reference position after annealing, more intense and narrower but there is no one preferential direction. In the case of 10 Pa pressure shift is small but there is a strong increase in intensity after argon annealing. Finally, samples deposited at oxygen pressure of 100 Pa do not show significant shift or change in intensity and have no preferential direction of growth (remind that they grow by cluster assembly). Generally, films annealed in argon atmosphere show better beahvior than that annealed in high vacuum.
In the same Figure also domain size D and lattice parameter c are shown. Except for the case of sample deposited at 0,1 Pa pressure and annealed in high vacuum, D has the same behavior for the three cases. It has maximum for 0,1 Pa pressure then, increasing pressure mean domain size decreases until 10 Pa pressure. At 100 Pa pressure it grows reaching agian a maximum. After annealing this parameter improves, especially for that in argon atmosphere, and it is quite similar for the three cases at 100 Pa pressure. This improvement could be do to an improved crystalline structure of films during

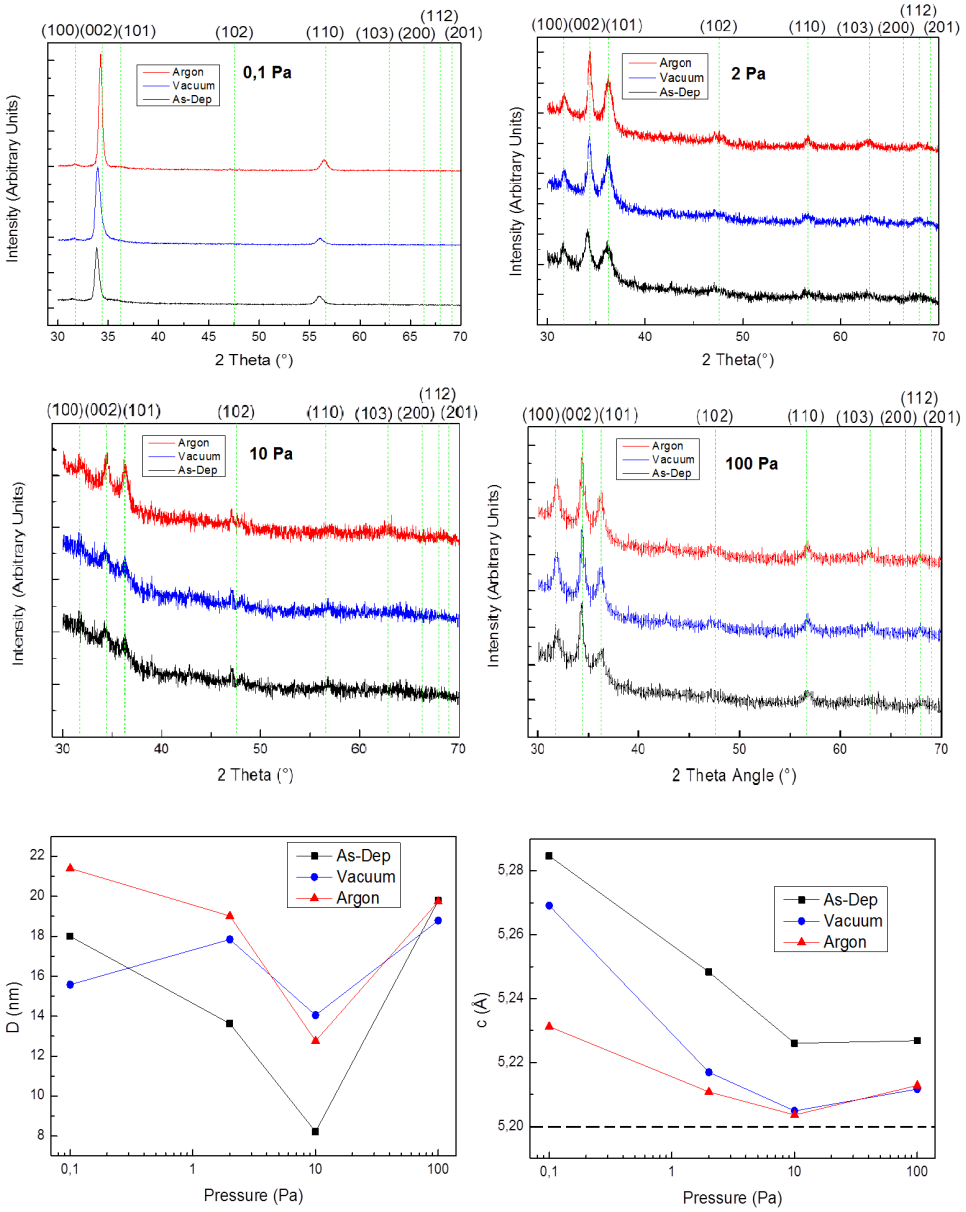

Figure 4.15: Top and middle: comparison of XRD spectra of samples deposited at different pressure between as deposited and annealed films. Dashed lines indicate reference peaks position for crystalline zinc oxide [45]. Bottom: comparison of mean domain size and reticular parameter. Dashed line is reticular parameter of crystalline zinc oxide [45].

the annealing that does not occur for sample deposited at 100 Pa pressure probably due to its tree-like nature.
Lattice parameter instead reduces after annealing. Its behavior is quite similar to that of as deposited samples, with a decrease with increasing pressure until 10 Pa and a *plateau* or a sligth increase at 100 Pa. Films annealed in argon atmosphere show a lower c already at 0,1 Pa pressure, especially for annealing in argon pressure. This could mean that there is a movement of aluminum and zinc ions from interstitial to substitutional position, especially for argon annealing, that reduces vertical dimension of the elementary cell. Also in this case zinc oxide reference value (5,2 Å) is not reached.

Raman analysis

In Figure 4.16 and 4.17 Raman spectra obtained with excitation wavelength respectively of 532 and 457 nm are shown. Films have a disordered Raman spectrum until 10 Pa deposition pressure. At 100 Pa pressure they become stoichiometric due to lower concentration of oxygen vacancies. After annealing all films show sharper and narrower peaks in reference position. This is an effect of reorganization of the ions seen also with XRD but could be also due to desorption of oxygen at grain boundaries discussed in section 4.2.1. Compact films remain substoichiometric. As a matter of fact the peak related to oxygen sublattice at 437 cm^{-1} (E_2^{high}) is a large band and becomes a peak only for sample deposited at 100 Pa.
For all samples the peak at 275 cm^{-1} after annealing appears, related to an anomalous mode. As seen in Section 4.2.1 these films are very conductive with high carrier density. This confirms the hypothesis discussed in Section 3.1.3 according to which this peak is related in some way to free charge carriers. This peak is more intense for samples annealed in vacuum that, as seen before, have a greater charge concentration with respect to those annelaed in argon atmosphere. Furthermore this anomalous mode appears also for sample deposited at 100 Pa oxygen pressure and then annealed. As a matter of fact, as seen in Section 4.2.1 also for porous film after annealing carrier density increases also for these films, confirming again the hypothesis about

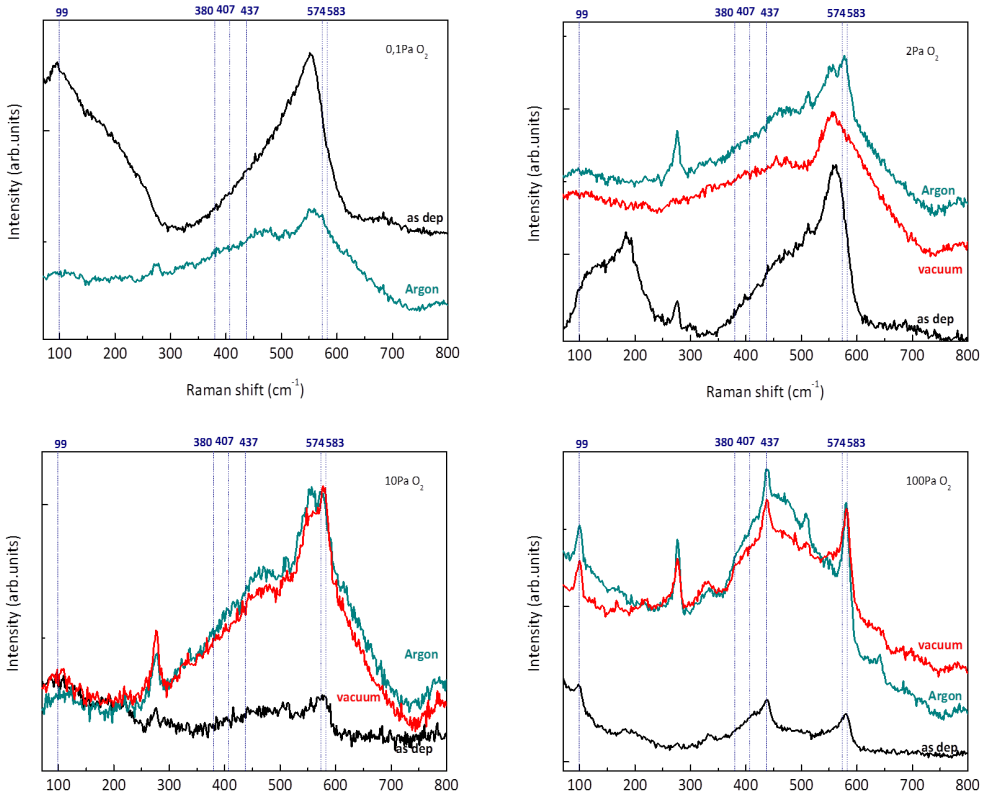

Figure 4.16: Comparison between Raman spectra of as-deposited and annealed film achieved with excitation wavelength of 532 nm.

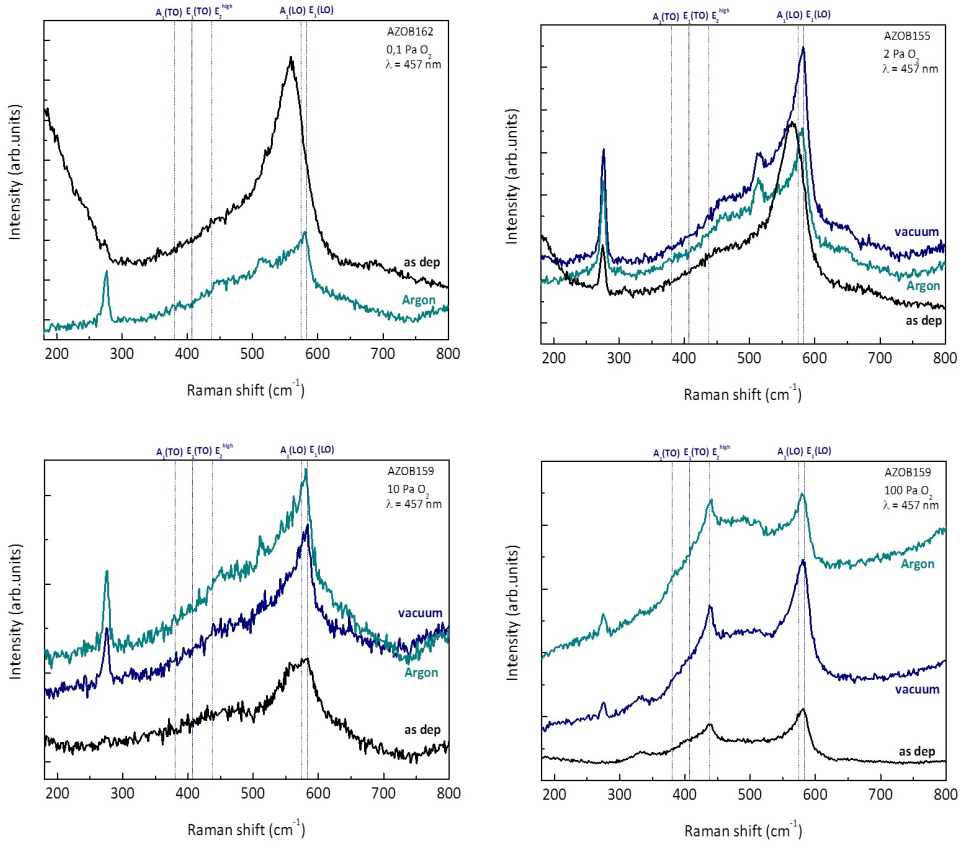

Figure 4.17: Comparison between Raman spectra of as-deposited and annealed film achieved with excitation wavelength of 532 nm.

rising of these anomalous mode.

4.3.2 Functional properties

Electrical measurements

In Figure 4.18 a comparison of electrical resistivity between as-deposited and annealed films is shown. As said before, 50 and 100 Pa sample as deposited

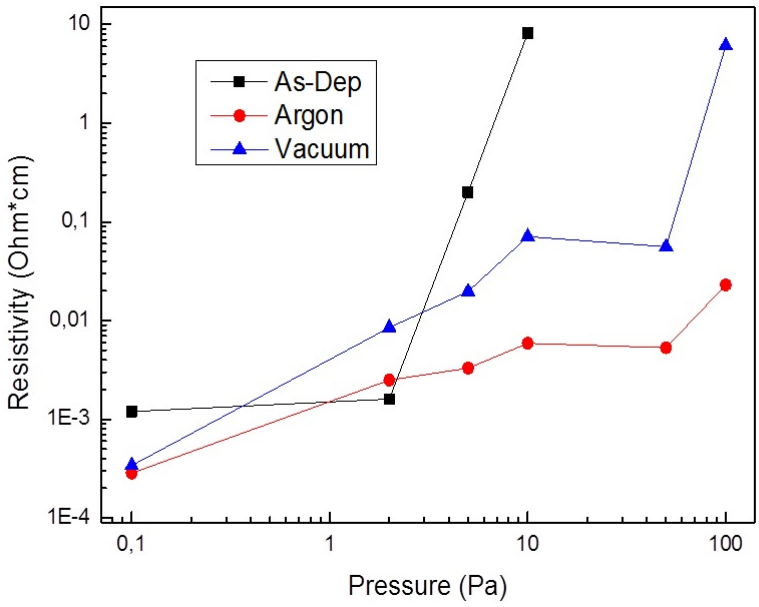

Figure 4.18: Comparison of resistivity between as-deposited and annealed film

result to be non conductive. On the contrary after annealing they show a quite low resistivity. Except for film deposited at 2 Pa oxygen pressure, all the samples show a great improvement in electrical conductivity. In the case of 10 Pa pressure annealed in argon it is even of three order of magnitude. Improvement are larger for annealing in argon atmosphere also in this case. This fact is in agreement with carrier density and mobility as can be seen in Figure 4.19. As deposited samples show a decreasing carrier concentration with increasing pressure. On the contrary, annealed films reaches rapidly a *plateau* until 50 Pa maintening n at an optimal value even at higher pressure.

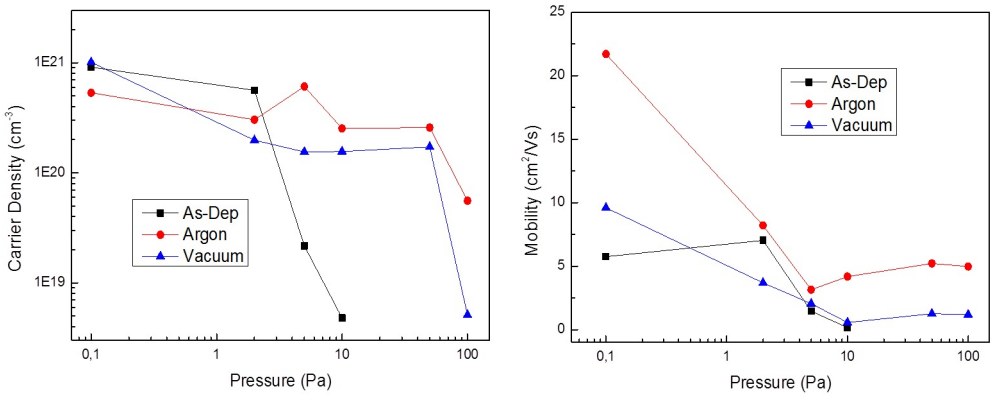

Figure 4.19: Comparison of carrier density (left) and mobility (right) between as-deposited and annealed film achieved with excitation wavelength of 532 nm.

In particular, samples annealed in argon atmosphere have a carrier density about between 2x10^{20} and 6x10^{20} cm^{-3}, optimal value that permits to have high mobility with high carrier concentration. Carrier density strongly decreases at 100 Pa pressure.

Also mobility improves after annealing. As-deposited samples show low μ, with a maximum at 2 Pa oxygen pressure and a decrease with increasing deposition pressure. Also in this case annealing in argon atmosphere results in better improvement with respect to high vacuum. In particuar a maximum value of mobility is reached for argon annealing of the sample deposited at oxygen pressure of 0,1 Pa. Combination of this with high density of carriers explains why minimum resistivity value is reached for this film. On the contrary, even if 0,1 Pa pressure sample has a high carrier concentration, mobility is low and ρ is greater than that after argon annealing.

Finally, possibility to increase μ with no change in carrier concentration for compact films permits to obtain more conductive samples without changing optical properties (Moss-Burnstein effect [20]).

Optical properties

In Figure 4.20 comparison between transmittance spectra of as-deposited and annealed film for different deposition pressure is shown. Porous films after

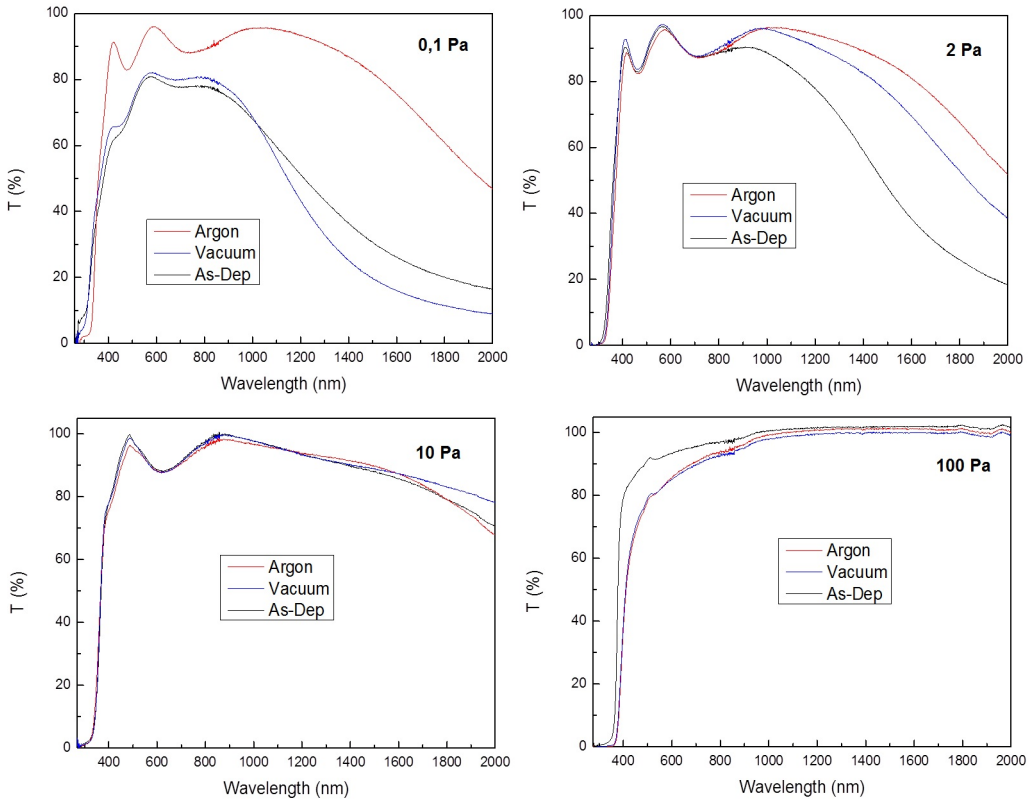

Figure 4.20: Comparison between transmittance spectra of as-deposited and annealed film for different deposition pressure. Transmittance spectra of porous sample have been done for film deposited at a slight high pressure, comparable with sample deposited at 100 Pa.

annealing undergo a slight decrease of transparency but still do not present interference fringes. On the contrary sample deposited at 10 Pa after annealing shows little changes in the visible range but in the case of annealing in high vacuum transmittance in the infrared region increases. Films deposited at an oxygen pressure of 2 Pa instead show a great increase of transparency in this region. For these samples carrier density decreases so this behavior

is justified with a lower density of free electrons that can support plasmonic oscillation. However, greatest changes are for film deposited at 0,1 Pa pressure. After annealing in high vacuum transmittance is slightly higher in visible range but falls in infrared region. As a matter of fact this sample has a greater carrier density. On the contrary, film annealed in argon atmosphere has lower charge concentration meaning higher transmittance in infrared region. In the visible range these spectra show well defined interference fringes becoming similar to that of film deposited at 2 Pa oxygen pressure. Also rising edge changes for this sample. This is related to lower concentration of defects in the optical gap (trap site) after annealing.

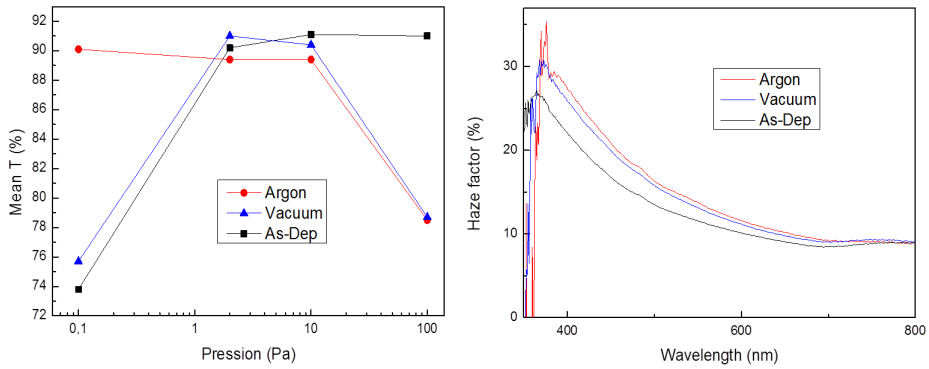

Figure 4.21: Mean transmittance (left) and haze factor (right)

In Figure 4.21 mean transmittance in the visible range is shown. It reflects behavior of transmittance spectra with significant improvement only for film deposited at 0,1 Pa oxygen pressure and annealed in argon atmosphere. Samples deposited at 2 Pa and 10 Pa pressure after annealing show little variation of at most 4%. Porous film instead undergoes a great decrease in transparency after annealing of about 15%. As a matter of fact, sample deposited at 0,1 Pa oxygen pressure is dark but after annealing in argon atmosphere becomes transparent while 2 Pa and 10 Pa pressure films do not change their color. Instead, 100 Pa pressure sample becomes darker after annealing but as-deposited it is white.

Finally, after annealing haze factor in the visible range increases. This could be do to the sintering of nanostructures creating larger but still scattering

grains.

4.4 Discussion and conclusions

All samples after annealing undergo deep structural changes. This effect is useful to understand the relation between morphology, structure and functional properties. The functional properties of the as deposited films obtained in this work are slightly different from literature. This is due to some problems with the deposition apparatus. The optimal case for electrical properties in this case is for the sample deposited at an oxygen pressure of 0,1 Pa in contrast with 2 Pa literature optimum [36].
Annealing post-deposition treatments strongly modifiy films structure. As a matter of fact, compact annealed films result more crystalline with larger mean domain size and lower vertical c parameter of the unit cell suggesting a possible improvement in crystallinity and a moving of interstitial atoms to substitutional positions. Improvements in these parameters are stronger for annealing in argon atmosphere than in high vacuum. Porous films do not present significantly changes in mean domain size but only in lattice parameter. Annealing does not significantly affect stoichiometry. As a matter of fact, for porous films Raman spectra reveal substoichiometric and local disordered films also after the treatment. No significant variations in films thickness have been observed but only a slightly better interconnetion.
These changes in structure reflect also in functional properties. Except for the sample deposited at a pressure of 2 Pa, compact films after annealing become more conductive. This effect is due to improvement both in mobility and in carrier density. In this work it has been seen that these two quantities are strongly related to structure and stoichiometry. First of all, the increase in crystalline domain size strongly affects mobility which in some cases increases by 100%. At the same time carrier density increases.This could be due to two different effects. First of all, during the annealing process lattice it is possible that oxygen desorption may occur. This would form some anionic vacancies behaving as two electrons donor. The second possible process is the migration of aluminum and zinc ions from interstitial to substitutional

position. Analyzing Raman spectra it can be seen that after annealing films become a little more stoichiometric. This means that the increase in carrier density is due to Al^{3+} and Zn^{2+} migration. This movement is suggested also by XRD analysis. As a matter of fact, lattice parameter decreases with respect to as-deposited samples, due to this migration that reduces vertical dimension of elementary cell. This increase in carrier density is visible also in optical spectra. As a matter of fact, if after annealing charge concentration increases, also absorption in infrared region improves. On the contrary, if n reduces, plasmonic effects decreases as for the case of sample deposited at a pressure of 0,1 Pa and then annealed in Ar atmosphere. Except for this one, compact films do not show big changes in mean transparency in the visible range.

The sample deposited at 2 Pa oxygen pressure is anomalous. As a matter of fact in literature it is the optimal one [36]. As said before in this work it was not possible to reach this value due to technical problems. However, it is interesting to analyze this case that combines good electrical properties with high optical qualities. First of all, this film is the only one that shows lower electrical properties after annealing. This is due to a little change of mobility but, at the same time, a decrease in carrier density. This fact is probably a consequence of saturation of oxygen vacancies due to presence of impurities, reducing free electrons. As a matter of fact, films become more stoichiometric as can be seen from Raman spectra where peaks are more defined. This decrease in carrier density reflects in optical properties. In the infrared range transmittance strongly increases because of reduction of plasmonic effects. Futhermore, mobility decreases even if mean domain size increases. This means that μ does not depend only on cristallinity. As discussed in Section 1.1.1 there are different scattering mechanisms for a TCO. One is interaction with dislocations and grain boundaries. Oxygen in this position behaves as a trap site for conduction electrons strongly reducing mobility. Also in this case the lattice parameter decreases after annealing because of ions migration.

Porous film result to be conductive after annealing. As a matter of fact, mobility at higher pressure seems to reach a *plateau* with a value of about

5 cm^2/Vs for samples annealed in Ar atmosphere. This improvement in μ is simultaneous to a good increase in carrier density making these films conductive with a value of ρ of about 10^{-2} Ωcm for annealing in argon atmosphere of film deposited at a pressure of 100 Pa.
It can be noted that the two different annealing environments differently modify the properties of the films. Even if high vacuum base pressure is reached, some air, low but not negligible, may remain in the oven during the annealing. Probably, residual oxygen saturates anionic vacancies making vacancy creation less effective (excluding porous films). This can be seen from Raman spectra from which annealed samples result more stoichiometric as said before. The two atmosphere clearly work differently. Probably, argon atmosphere is more pure and prevents oxygen migration to the samples. As a matter of fact, generally better improvements are for annealing in argon atmosphere.
Finally, it must be taken in mind that also hydrogen may play a role in carrier density. It has been theoretical studied that it affects functional properties of the films. Hydrogen is difficult to remove completely from the oven also at high vacuum. So, it may smoothly migrate in the film modyfing its properties. To preliminary study hydrogen effects an annealing in mixed atmosphere (3% H_2-97% Ar) has been done. In this work only electrical characterization was performed and the results are reported in Section 5.1.
Summarizing, some conclusions can be drawn.

- First of all, there are strong correlations between morphology, structure and functional properties. Compact films present good electrical properties. This is due to combination of high mobility and good carrier density. On the contary, porous films are very resistive because of their low charge concentration and poor interconnection between different structures.

- Mobility depends mainly on mean domain size, defects and oxygen at grain boundaries.

- Carrier density depends on oxygen stoichiometry and substitutional ions. During annealing migration of interstitial to substitutional ions

strongly improves charge concentration even if there is saturation of some anionic vacancies.

- Optical properties are influenced by morphology, conduction electrons and oxygen vacancies. As a matter of fact, compact films are transparent but do not scatter light. On the contrary, porous samples have a high haze factor that permits to trap light. Furthermore, high concentration of conduction electrons reduces transparency in the infrared region while defect levels reduce the optical gap.

- Annealing is a good technique to improve electrical properties without affecting optical ones. This because it is able to increase the crystallinity of the film increasing mobility and to move ions to substitutional position improving carrier density. It is clear that this technique can be used only if the other components of the device using AZO resist to high temperature.

- Finally, a deeper study about hydrogen effects has to be done on this material to know how it may affect functional properties.

Chapter 5

Preliminary and related experiments

The purpose of this work was to found the relationship between morphology, structure and functional properties of AZO as a function of post deposition annealing processes. During this time I have also done some preliminary experiments linked to that of Chapter 4. In particular I have done annealing in Ar:H_2 atmosphere and annealing on an old optimized sample in argon atmosphere. Finally, I took part at others activity with aim of develop new AZO nanostructures. In this chapter these side works will be presented.

5.1 Annealing in Argon-Hydrogen atmosphere

To preliminary investigate the possible role of hydrogen, annealing in mixed Ar:H_2 atmosphere of Aluminum-doped Zinc Oxide films was performed. As a matter of fact there are some works (in particular theoric works) in literature wich say that hydrogen, which is always present also at high vacuum, plays a role in electrical properties of AZO. The atmosphere used is a mixture composed of 3% of hydrogen and 97% of argon. Annealing was done using the same parameters described in section 2.4 with a slow temperature ramp. Also in this case three subsequent gas injection were done after reaching base pressure of about $3x10^{-5}$ Pa to purify the chamber. Annealing pro-

cedure has been done only on thick samples to allow subsequent structural analysis with XRD and Raman scattering. This work have been done at he end of the thesis work so only elctrical properties have been investigated. Resistivity results are in Figure 5.1. Measures have been done on thicker samples, comparable to results obtained in Chapter 4. It is easy to see that

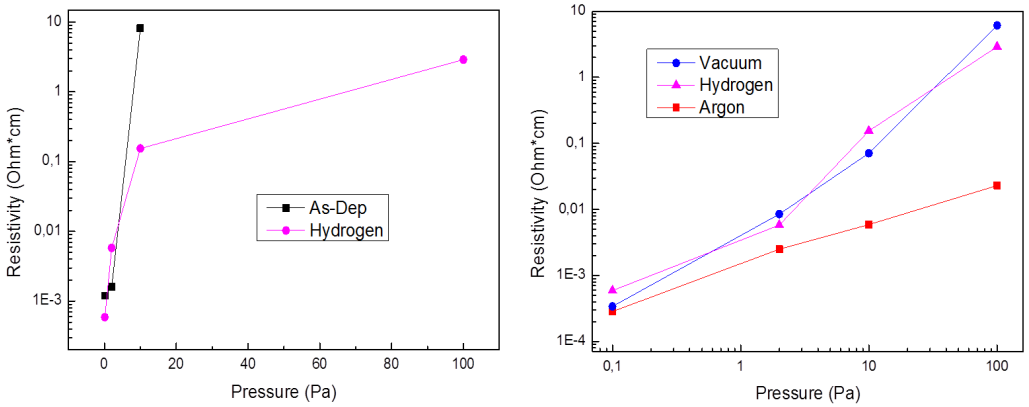

Figure 5.1: Resistivity versus deposition pressure for films annealed in mixed atmosphere. On the left: comparison with as-deposited samples. On the right: comparison with films annealed in high vacuum.

there is a good improvement compared to as-deposited samples. Also in this case the only sample whose conductivity decreases is that deposited at 2 Pa oxygen pressure. Comparing resistivity of these samples it can be observed that their behavior is very similar to that of films annealed in high vacuum. Also carrier density and mobility were calculated (Figure 5.2). Carrier density is worse with respect to that of films annealed in argon atmosphere and high vacuum. It is similar until 2 Pa oxygen pressure but starts to decrease from 10 Pa pressure, contrary to the other types of annealing for which there is a *plateau* until 50 Pa. Also in this case the worst case is for films deposited at 100 Pa (initially more stoichiometric).
Mobility, instead, shows intermediate values between those of samples annealed in high vacuum and in argon atmosphere except for film deposited at 100 Pa oxygen pressure.
To understand this behavior further analysis must be done as X-Ray Diffrac-

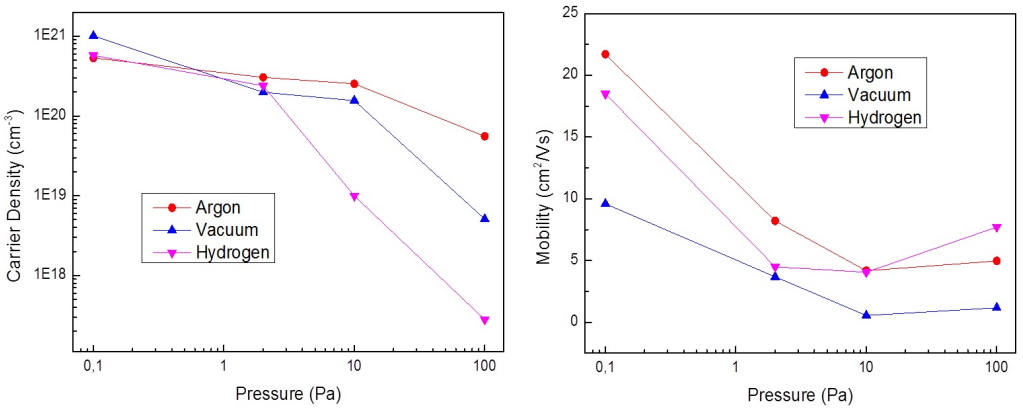

Figure 5.2: Comparison of carrier density (left) and mobility (right) between films annealed in different atmospheres.

tion, Raman spectroscopy and optical measurements but also X-ray Photoelectron Spectroscopy (XPS) that allows to study local chimical environment.

5.2 Annealing on old sample

As seen in section 3, samples deposited in this work were not electrical optimized. As a matter of fact, resistivity results greater than values in literature [36][24] for which the optimal case is for film deposited at oxygen pressure of 2 Pa. So, an annealing in high vacuum and in argon atmosphere have been done on an old sample, optimized in terms of conductivity, deposited two years ago to as a comparison with samples of this work. First of all it was verified that structural and electrical properties of the as deposited sample did not significantly change in time (24 months). Then, films have been annealed as samples discussed in chapter 4 and studied with Raman spectroscopy, Van der Pauw method and Hall measurements. Raman results are shown in Figure 5.3. Also these analysis confirm the results on the samples deposited at 2 Pa pressure discussed in this thesis. As a matter of fact annealed samples have no relevant peak related to the oxygen sublattice. Furthermore, also in this case peak at 275 cm^{-1} appears and increases after annealing.

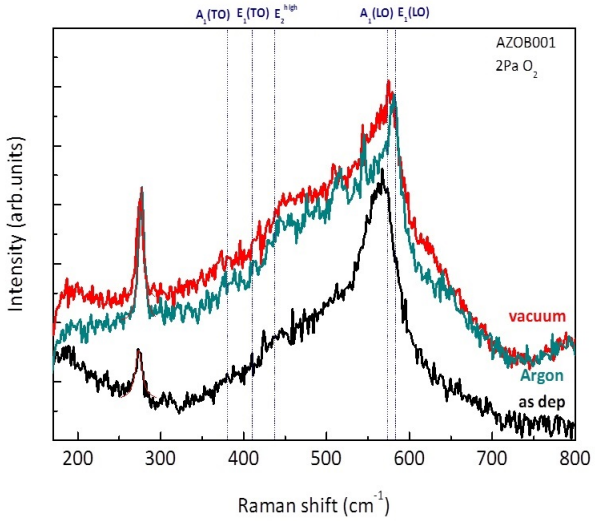

Figure 5.3: Comparison between Raman spectra of old as-deposited and annealed film achieved with excitation wavelength of 457 nm.

Table 5.1: Electrical properties of old film before and after different annealing.

Sample	Resitivity	Carrier density	Mobility
As-deposited	2,27 x10^{-4}	9,1 x10^{20}	31,0
High vacuum	2,05 x10^{-4}	1,1 x10^{21}	27,5
Argon	2,73 x10^{-4}	7,3 x10^{20}	32,1

In Table 5.1 electrical properties before and after different annealing are shown. Resistivity is very similar for all three cases. This because for annealed samples variation in carrier density is compensated by variation in mobility. As a matter of fact, for annealing in high vacuum n increases but μ decreases. On the contrary, the film annealed in argon atmosphere has a higher mobility but a smaller carrier density. These results are similar to that obtained for films deposited at 0,1 Pa. As a matter of fact this sample is the new optimal one.

This is just a preliminar analysis. Final target is to obtain optimal films at every deposition pressure and study what happens during annealing proce-

dure with all the techniques used in this work.

5.3 Graded films

As seen before, compact films have good electrical properties while porous ones have high optical qualities (e.g. haze factor). The idea of graded films is to combine these two characteristics in the same layer. Two different types of graded films can in principle be grown as shown in Figure 5.1. The first

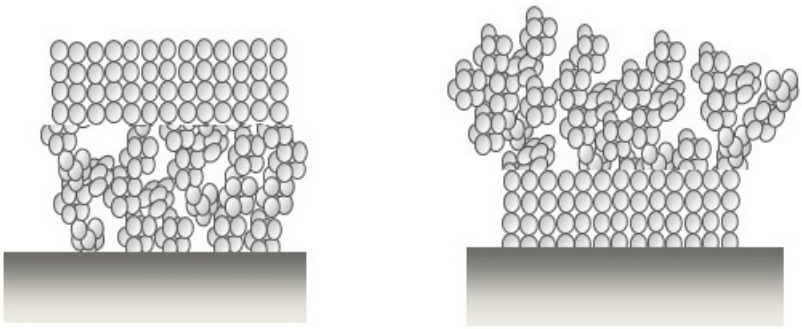

Figure 5.4: Different type of graded films.

one (on the left) consists in a compact film over a porous one, the other is built viceversa. The aim is to have a conductive but also scattering (for light trapping in active material) electrode on which building a cell. If compact layer is below film does not conduce current.
These type of structures are deposited in three steps. First of all porous part is deposited with high oxygen pressure in the chamber (tipically between 100 and 200 Pa). Then, pressure is decreased gradually until reaching the desired value for the compact conducting layer between 0,1 and 3 Pa. Finally it is maintained constant to grow the compact layer. In this way resulting structures are stable with no relevant residual stress and there is strong interaction between porous and compact layer. Compact layer must be not too thin to be conductive but not too thick to be transparent while the other layer must be porous to scatter light but not too much to have high

transmittance and good connectivity of compact layer. In Figure a 5.5 SEM a image of typical graded structure is shown. These types of films have a

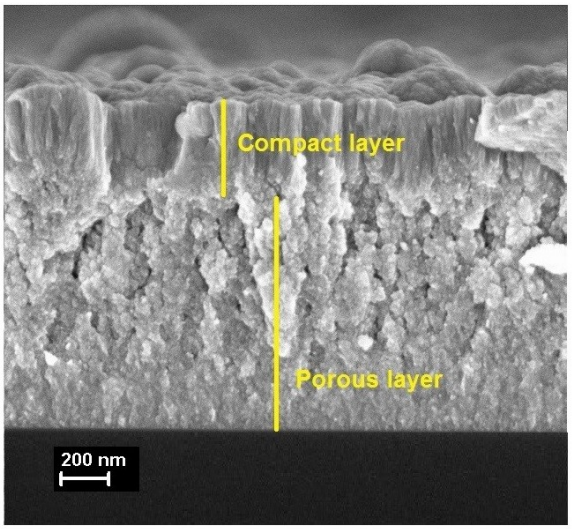

Figure 5.5: SEM image of graded film.

resistivity of 3 mΩ cm with transmittance of about 80% and haze factor of 40%. These values are good but structure must be optimized. The reason can be understood also from SEM images. As a matter of fact, the compact layer, that must be responsible of electric conduction, follow the morphology of the porous structure below. So, it results more disordered and less interconnected films grown on flat substrates.

Chapter 6

Conclusions and perspectives

The aim of this thesis work was to study the correlation between morphological, structural and functional properties of nanostructured Aluminum-doped Zinc Oxide films. Samples have been prepared with Pulsed Laser Deposition technique and the structure has been controlled by changing the oxygen pressure in the chamber during deposition. Resulting films have different morphologies, compact at low deposition pressure, tree-like and nanoparticle-assembled at high deposition pressure. Samples for every deposition condition have been annealed in high vacuum and in argon atmosphere at 500 °C for 1 hour. Both as deposited samples and annealed films have been characterized. Morphology was observed using Scanning Electron Microscopy while cristallinity and stoichiometry were investigated with X-Ray Diffraction and Raman spectroscopy. Electrical properties, in particular resistivity, carrier density and mobility, have been studied with Van der Pauw method and Hall effect measurements and optical properties (transperency and haze factor) using a UV-vis-NIR spectrophotometer.
Strong correlations between morphology, structure and functional properties have been observed. As a matter of fact, compact films have good electrical properties due to combination of high mobility and good carrier density. On the contary, porous films are slightly interconnected and are characterized by a low carrier density, so they are very resistive. Furthermore, mobility depends mainly on cristallinity, defects and oxygen at grain boundaries (that

works as trap site). Instead, carrier density depends on stoichiometry (oxygen vacancies) and substitutional ions (aluminum doping).
Optical properties are influenced by morphology, conduction electrons and oxygen vacancies. Haze factor, that is the ability to scatter light, depends on the presence of structures at the nanometer and sub-micrometer scale as they are built cluster by cluster. On the contrary compact films shows high transparency with interference fringes. Instead, transparency in infrared region is influenced by conduction electrons and optical gap reduces upon increasing defects and in particular oxygen vacancies.
Annealing is a good technique to improve electrical properties without affecting optical ones. This because during it films become more crystalline. Moreover we suggest that annealing is beneficial for moving interstitial ions to substitutional position improving carrier density. This increasing in n is not so strong to affect transparency in the infrared region. Clearly, this technique can be used only if the substrate of the device using Aluminum-doped Zinc Oxide can resist to high temperature. Results obtained on functional properties confirm that AZO is an optimal substitute of more expensive and pollutant Indium Tin Oxide. As a matter of fact in the best case transparency is around 90% with a resistivity of about 10^{-4} Ωcm, comparable with that of ITO [1]. Improvement are greater for annealing in argon atmosphere than for annealing in high vacuum. Moreover, all electrical properties of the films improve except for sample deposited at 2 Pa. Compact films show also improved optical properties.
Some questions are still open and require more studies and further experiments. First of all a deeper study to understand what happens at structural level due to annealing is necessary. Some techniques like X-ray Photoemission Spectroscopy (XPS) are sensible to atoms chemical environment. They could give some information about changes in doping, vacancies, interstitial and substitutional atoms during the annealing. The strange behavior of the sample deposited at an oxygen pressure of 2 Pa could be object of extensive investigation. Even if it is the optimal film for old samples as reported in the literaure (see Section 5.2), after annealing its electrical properties worsen while the other samples show an opposite behavior. Another open issue is

the role of hydrogen. To understand how it affects films properties a good way is to do annealing in a mixed atmosphere with a high percentage of hydrogen. Furthermore, detailed Raman studies could be performed to expand the knowledge for the AZO system (still limited) and to understand some anomalous features in Raman spectra like the peak at 275 cm^{-1}.
All depositions have been done at room temperature. So, another way to study the correlation between structure and functional properties is to do high temperature deposition. This would allow also a comparison between this technique and annealing. Finally, annealing with different times and temperatures could be done on this material to understand how these parameters affect structure and stoichiometry.
All of these studies will allow a deep understanding of AZO nanostructures and mechanisms that rule functional properties, relevant for technological application, in order to improve them.

Bibliography

[1] T. Minami *Semicond. Sci. Tech. 20*, 35-44 (2005)

[2] E. Fortunato, D. Ginley, H. Hosono and D. C. Paine, *MRS Bulletin 32*, 242-247 (2007)

[3] D. S. Ginley and C. Bright, *MRS Bulletin 25*, 15-18 (2000)

[4] C. G. Granqvist, *Solar Energy Materials 91*, 1529-1598 (2007)

[5] A. Banerjee and K. Chattopadhyay, *Progress in Crystal Growth and Characterization of Materials* (2005)

[6] Edwards et al., *Dalton Transactions* (2004), 2995-3002

[7] J. Fan and J. Goodenough *Journal of Applied Physics 48*(8), 3524-3531 (1977)

[8] I. Kiliç and A. Zunger, *Phys. Rev. Lett. 88*(9), 095501 Feb (2002)

[9] N. Mott *Journal of Solid State Chemistry 88*(1), 5-7 (1990)

[10] N. W. Ashcroft and D. N. Mermin *Solid State Physics*, Thomson Learning, Toronto, January (1976)

[11] U. Özgür et al. *Journal of Applied Physics 98*, 1-103 (2005)

[12] K. Ellmer, *Journal of Physics D: Applied Physics 34*, 3097-3108 (2001)

[13] K. Miyamoto, M. Sano et al. *Japanese Journal of Applied Physics 41*, L1203-L1205 (2002).

[14] vExharos et al., *Thin Solid Films 515* 7025-7052 (2007)

[15] G. Thomas, *Nature 389*, 907-98 (1997)

[16] K. Narasimhan et al., *Thin Solid Films 295*, 104-106 (1997)

[17] J. C. Manifacier, J. Gasiot and J. P. Fillard, *Journal of Physics E: Scientific Instruments 9*, 1002-1004 (1976)

[18] J. Seong and D. Y. Kim, *Journal of the Korean Physical Society 54* (6), 2396-2399 (2009)

[19] J. Tauc, *Materials Research Bulletin 3*, 37-46 (1968)

[20] L. Burstein, *Physical Review 93*, 632-633 (1954)

[21] B. Sernelius, *Phys. Rev. B 37*(17), 10244-10248 (1988)

[22] T. J. Coutts and D. L. Young, *MRS Bulletin 25*, 58-65 (2000)

[23] T. Minami, *Thin Solid Films 517*, 1474 - 1477 (2008)

[24] P. Gondoni, M. Ghidelli, F. Di Fonzo, M. Carminati, V. Russo, A. Li Bassi and C. S. Casari, *Nanotechnology* 23 *(2012) 365706 (8pp)*

[25] M. Graetzel and J.R. Durrant, *World Scientific*

[26] A. B. F. Martinson et al., *Nano Letters 8* (9), 2862-2866 (2008)

[27] A. B. F. Martinson et al., *Journal of Physical Chemistry A 113* (16), 4015-4021 (2009)

[28] A. Jain, P. Sagar, R. M. and Mehra, *Solid-State Electronics 50*, 1420-1424 (2006)

[29] C. Kittel, *Introduction to solid state physics* Wiley, New York, 5th ed. edition, (1976)

[30] C. Agashe, O. Kluth et al., *Journal of Applied Physics 95* (4), 1911-1917 (2004)

[31] J.Herrero and C. Guillén, *Vacuum 84*(7), 924-929 (2010)

[32] N. M. Sbrockey and S. Ganesan, *III-Vs Review 17*(7), 23-25 (2004)

[33] R. Romero, R. López-Ibáñez et al., *Journal of Physics D: Applied Physics 43*(9), 095303 March (2010)

[34] C. Benouis, A. Sanchez-Juarez and M. J. Aida, *Applied Sci. 7*, 220-225 (2007)

[35] Carlo S. Casari and Andrea Li Bassi, *Pulsed Laser Deposition of nanostructured oxides: from cluster to functional films*, in *Advances in Laser and Optics Research. Volume 7*, edited by William T. Arkin, Nova Science Publishers, (2011), pp. 65-100

[36] P. Gondoni, M. Ghidelli, F. Di Fonzo, V. Russo, P. Bruno, J. Martí-Rujas, C.E. Bottani, A. Li Bassi, C.S. Casari, *Thin Solid Films 520* (2012) 4707–4711

[37] F. Ruske, M. Roczen, K. Lee, M. Wimmer et al., *Journal of Applied Physics 107*, 013708 (2010)

[38] M. Wimmer, F. Ruske, S. Sherf, B. Rech, *Thin Solid Films 520* 4203-4207 (2012)

[39] M. Warzecha, J. I. Owen, M. Wimmer, F. Ruske, J. Hotovy and J. Hupkes, *Materials Science and Engineering 34* 012004 (2012)

[40] Byeong-Yun Oh, Min-Chang Jeong, Doo-Soo Kim, Woong Lee and Jae-Min Myoung, *Journal of Crystal Growth 281* 475-480 (2005)

[41] Xuhu Yu, Jin MaT, Feng Ji, Yuheng Wang, Xijian Zhang and Honglei Ma, *Thin Solid Films 483* 296– 300 (2005)

[42] M. Fusi, *Titanium oxide nanostructured surfaces for biotechnology applications*, Politecnico di Milano, 2009

[43] L. J. Van der Pauw, *Philips Research Reports 13(1)*, 1-9 (1958)

[44] C. Kelley, *Solving Nonlinear Equations with Newton's Method*, Society for Industrial and Applied Mathematics, Philadelphia, (2003)

[45] http://database.iem.ac.ru/mincryst/

[46] B. Z. Dong, H. Hu, G. J. Fang, X. Z. Zhao, D. Y. Zheng, Y. P. Sun, *Journal of Applied Physics*, *103*, 2008

[47] T. C. Damen, S. P. S. Porto, B. Tell, *Physical Reviews 142* (1966) 570

[48] N. Ashkenov et al., *Journal of Applied Physics* Volume 93, Number 1, 2003

[49] M. Tzolov, N. Tzenov, D. Dimova-Malinovska, M. Kalitzova, C. Pizzuto, G. Vitali, G. Zollo, I. Ivanov, *Thin Solid Films 379*, 2000, 28-36

[50] C. Kelley, *Solving Nonlinear Equations with Newton's Method*, Society for Industrial and Applied Mathematics, Philadelphia, (2003)

[51] P. Gondoni, *Proprietà ottiche e di trasposrto elettrico di film di ZnO drogato Al per applicazioni fotovoltaiche*, thesis work, Politecnico di Milano, 2010

Ringraziamenti

Arrivato alla fine di questo lavoro (quasi un'impresa per il mio inglese scritto, notevolmente migliorato sul finire della tesi) posso finalmente scrivere in maniera impersonale e, soprattutto, in italiano, lingua non molto parlata nel Mondo ma che ha regalato alla storia capolavori come la Divina Commedia, le poesie di Ungaretti e le canzoni di Cesare Cremonini (anch'esse pura poesia).
Innanzitutto, il mio più grande ringraziamento va ai miei genitori. Non solo per il loro sostegno economico senza il quale non sarei potuto arrivare a questo traguardo, ma soprattutto per avermi donato la vita ed averla resa meravigliosa. Chi mi conosce sa che sono una persona molto ottimista (forse anche troppo)...questo lo devo a loro, ai loro insegnamenti, alla loro presenza, alla dolcezza di mia madre ed alla forza di mio padre. Grazie. Davvero. Mi viene in mente una frase di una canzone (leggermente parafrasata): "So che ogni cosa la devo alle spalle di mio padre, al suo sudore, al sorriso di mia madre, al viso di ogni nonno che proietta amore".
Il secondo ringraziamento (non me ne vogliano ma il primo è sempre alla famiglia) va al mio relatore, prof. Andrea Li Bassi, e al mio correlatore, ing. Paolo Gondoni, per la loro infinita disponibilità e pazienza. Sono stati sempre disponibili (quasi ai limiti dell'impossibile) ad aiutarmi e ad ampliare le mie conoscenze. Un ringraziamento particolare ad Andrea per il lavoro titanico di correzione della mia tesi (compito per nulla semplice) e a Paolo per il suo aiuto: come gli ho detto una volta, è fatto per insegnare. Ringrazio inoltre anche la dott.ssa Valeria Russo per la sua disponibilità nelle analisi Raman e l'ing. David Dellasega per l'aiuto con l'XRD e per qualsiasi altro problema.

Un altro ringraziamento va a tutto il gruppo di NanoLab per avermi dato la possibilità di svolgere il mio lavoro di tesi in questo dipartimento e, cosa ancora più importante, per avermi fatto sentire come a casa. Mi ricorderò sempre quando il Maffo, dopo solo due giorni che lavoravo in laboratorio, mi ha invitato a giocare a calcetto con loro. Quando si è sereni si lavora molto meglio. Di conseguenza grazie a Piero (grazie per il tuo aiuto ed i tuoi consigli), Maffo, Andreino, Ale Zani, Andrea e Paolo Carrozzo e gli ing. Carlo Casari (anche lui mi ha spesso seguito ed aiutato) e l'ing. Matteo Passoni.
Sempre in ambito tesi devo ringraziare le persone che hanno reso quest'ultimo anno indimenticabile. Il primo ringraziamento va a Fede, Edo e Lorenzo, bomber veri. Non pensavo che sarei riuscito a trovarmi così in sintonia con alcune persone in così poco tempo. D'altronde come si fa a non divertirsi con voi? Grazie ragazzi, siete più forti addirittura di Moscardelli! Un grazie anche a Gianfranco Palacio, Bertoc e Sam per le ore passate insieme.
Rimanendo in ambito universitario invece voglio ringraziare alcune persone che mi hanno accompagnato in questi anni: Michi e Reno che hanno reso la triennale più "sopportabile". Ma il ringraziamento "universitario" più grande va ad Ale Piotto...anche se quest'anno ha deciso di abbandonarmi per sei mesi per andare in America, rimane sempre un amico unico, leale, sempre presente e sorridente. Grazie Ale per questi anni (anche se so che leggerai questi ringraziamenti in ritardo). Con te non ci si annoia mai!
In ambito scuola un ringraziamento particolare va anche ai miei ex compagni del Liceo dell'indimenticabile 5 I. Grazie a tutti voi: Bozzo (ed insieme a lui a tutti gli White Skulls), Colo, Roby, Eri, Ga, Deni, Cha, Sara e Vivi.
Ritornando alla famiglia, un ringraziamento per il loro supporto e per la loro allegria va alla mia splendida sorella Daniela ed ai miei due angeli, i miei nipotini (anche se uno non più così ino) Mattia ed Arianna. Vi voglio bene.
Ed un pensiero va anche alle mie due nonne, Lina e Giannina, che avrebbero voluto essere qui oggi ma so che fanno il tifo per me da lassù.
Uno dei ringraziamenti più speciali va invece ai miei amici di sempre. Se qualcuno vi dovesse dire che un ingegnere non ha amici non credetegli...io ne ho trovati di unici. Grazie Roby, Luca, Chicco, Tia, Marta, Lilli, Fede Tammy, Tai, Seba, Dani, Gesu, Sere e Cristian (con la piccola Emma), Marvy, Gatto,

Kirill, Albo, Fabi, Micio, Gabri, Casta, Ele, tutta la mitica squadra del CSI (mister e dirigenti compresi) e chiunque abbia dimenticato (chiedo perdono per questo). Grazie ragazzi...senza di voi probabilmente sarei impazzito. Ora si festeggia!!

Infine l'ultimo ringraziamento va a te Fede...a te che mi hai cambiato in meglio...a te che mi hai sorretto in questi anni...a te che mi hai fatto tornare la voglia di studiare quando l'avevo persa...a te che ogni giorno sei sempre vicina a me. Qualunque cosa accada, so che tu sei sempre lì. Penso non sia facile trovare la persona giusta che ci accompagni nella vita...io credo di aver trovato quella perfetta. Questa tesi è anche tua. Ti amo. Grazie a te che sei, semplicemente sei, sostanza dei giorni miei, sostanza dei sogni miei...

Ed un ringraziamento, perchè no, anche a me stesso per tutto il mio studio (anche se non ci crede nessuno, ho studiato un sacco) e per questo lavoro. Bravo Marco, sono fiero di te!!